

**Research Articles: Systems/Circuits**

**Network architecture underlying basal autonomic outflow: Evidence from frontotemporal dementia**

Virginia E. Sturm<sup>1</sup>, Jesse A. Brown<sup>1</sup>, Alice Y. Hua<sup>2</sup>, Sandy J. Lwi<sup>2</sup>, Juan Zhou<sup>3</sup>, Florian Kurth<sup>4</sup>, Simon B. Eickhoff<sup>5,6</sup>, Howard J. Rosen<sup>1</sup>, Joel H. Kramer<sup>1</sup>, Bruce L. Miller<sup>1</sup>, Robert W. Levenson<sup>2</sup> and William W. Seeley<sup>1,7</sup>

<sup>1</sup>Department of Neurology; University of California, San Francisco; Sandler Neurosciences Center; 675 Nelson Rising Lane, Suite 190; San Francisco, CA 94158, USA.

<sup>2</sup>Department of Psychology, University of California, 3210 Tolman Hall #1650, Berkeley, CA 94720-1650, USA.

<sup>3</sup>Center for Cognitive Neuroscience, Neuroscience and Behavioral Disorders Program, Duke-National University of Singapore Medical School, 8 college road, Singapore, Singapore 169857.

<sup>4</sup>Cousins Center for Psychoneuroimmunology, Semel Institute for Neuroscience and Human Behavior, Department of Psychiatry and Biobehavioral Sciences, UCLA School of Medicine, Medical Plaza 300, Los Angeles, CA 90095, USA.

<sup>5</sup>Institute of Systems Neuroscience, Medical Faculty, Heinrich Heine University Düsseldorf, Düsseldorf, Germany

<sup>6</sup>Institute of Neuroscience and Medicine, Brain & Behaviour (INM-7), Research Centre Jülich, Jülich, Germany

<sup>7</sup>Department of Pathology, University of California, San Francisco, CA 94143, USA.

DOI: 10.1523/JNEUROSCI.0347-18.2018

Received: 5 February 2018

Revised: 23 August 2018

Accepted: 27 August 2018

Published: 4 September 2018

**Author contributions:** V.E.S., R.W.L., and W.W.S. designed research; V.E.S., J.A.B., A.Y.H., S.J.L., J.Z., F.K., S.B.E., H.J.R., J.H.K., and B.L.M. performed research; V.E.S., J.A.B., J.Z., F.K., and S.B.E. analyzed data; V.E.S. wrote the first draft of the paper; V.E.S., J.A.B., A.Y.H., S.J.L., J.Z., F.K., H.J.R., J.H.K., B.L.M., R.W.L., and W.W.S. edited the paper; V.E.S., R.W.L., and W.W.S. wrote the paper.

**Conflict of Interest:** The authors declare no competing financial interests.

This project was supported by grants from the NIH National Institute on Aging (P50AG023501, P01AG019724, R01AG052496, R01AG032306, R01AG057204, 1K23AG040127, and 1K23AG045289), The Larry L. Hillblom Foundation (2013-A-029-SUP and 2005/2T), the John Douglas French Foundation; the Consortium for Frontotemporal Dementia Research, and the Tau Consortium. We are grateful for the patients, healthy controls, and families that have participated in our research studies.

Corresponding Author: William W. Seeley, M.D., UCSF Memory and Aging Center - Box 1207, Sandler Neurosciences Center, 675 Nelson Rising Lane, Suite 190, San Francisco, CA 94158, Phone: (415) 476-2793 Fax: (415) 476-0213

**Cite as:** J. Neurosci ; 10.1523/JNEUROSCI.0347-18.2018

**Alerts:** Sign up at [www.jneurosci.org/cgi/alerts](http://www.jneurosci.org/cgi/alerts) to receive customized email alerts when the fully formatted version of this article is published.

# AUTONOMIC NETWORK ARCHITECTURE

Running Title: AUTONOMIC NETWORK ARCHITECTURE

## Network architecture underlying basal autonomic outflow: Evidence from frontotemporal dementia

Virginia E. Sturm<sup>1</sup>

Jesse A. Brown<sup>1</sup>

Alice Y. Hua<sup>2</sup>

Sandy J. Lwi<sup>2</sup>

Juan Zhou<sup>3</sup>

Florian Kurth<sup>4</sup>

Simon B. Eickhoff<sup>5,6</sup>

Howard J. Rosen<sup>1</sup>

Joel H. Kramer<sup>1</sup>

Bruce L. Miller<sup>1</sup>

Robert W. Levenson<sup>2\*</sup>

William W. Seeley<sup>1,7\*</sup>

<sup>1</sup> Department of Neurology; University of California, San Francisco; Sandler Neurosciences Center; 675 Nelson Rising Lane, Suite 190; San Francisco, CA 94158, USA.

<sup>2</sup> Department of Psychology, University of California, 3210 Tolman Hall #1650, Berkeley, CA 94720-1650, USA.

<sup>3</sup> Center for Cognitive Neuroscience, Neuroscience and Behavioral Disorders Program, Duke-National University of Singapore Medical School, 8 college road, Singapore, Singapore 169857.

<sup>4</sup> Cousins Center for Psychoneuroimmunology, Semel Institute for Neuroscience and Human Behavior, Department of Psychiatry and Biobehavioral Sciences, UCLA School of Medicine, Medical Plaza 300, Los Angeles, CA 90095, USA.

<sup>5</sup> Institute of Systems Neuroscience, Medical Faculty, Heinrich Heine University Düsseldorf, Düsseldorf, Germany

## AUTONOMIC NETWORK ARCHITECTURE

<sup>6</sup>Institute of Neuroscience and Medicine, Brain & Behaviour (INM-7), Research Centre Jülich, Jülich, Germany

<sup>7</sup>Department of Pathology, University of California, San Francisco, CA 94143, USA.

\* authors contributed equally to the work

Corresponding Author:  
William W. Seeley, M.D.  
UCSF Memory and Aging Center - Box 1207  
Sandler Neurosciences Center  
675 Nelson Rising Lane, Suite 190  
San Francisco, CA 94158  
Phone: (415) 476-2793 Fax: (415) 476-0213

Number of pages: 53  
Number of figures: 5  
Number of tables: 5  
Number of words (Abstract): 250  
Number of words (Introduction): 647  
Number of words (Discussion): 1511

Conflict of interest: None

Acknowledgements: This project was supported by grants from the NIH National Institute on Aging (P50AG023501, P01AG019724, R01AG052496, R01AG032306, R01AG057204, 1K23AG040127, and 1K23AG045289), The Larry L. Hillblom Foundation (2013-A-029-SUP and 2005/2T), the John Douglas French Foundation; the Consortium for Frontotemporal Dementia Research, and the Tau Consortium. We are grateful for the patients, healthy controls, and families that have participated in our research studies.

## Abstract

65

66 The salience network is a distributed neural system that maintains homeostasis by regulating  
67 autonomic nervous system activity and social-emotional function. Here we examined how  
68 within-network connectivity relates to individual differences in human (including males and  
69 females) baseline parasympathetic and sympathetic nervous activity. We measured resting  
70 autonomic nervous system physiology in 24 healthy controls and 23 patients with behavioral  
71 variant frontotemporal dementia (bvFTD), a neurodegenerative disease characterized by baseline  
72 autonomic deficits. Participants also underwent structural and task-free functional magnetic  
73 resonance imaging. First, we used voxel-based morphometry to determine whether salience  
74 network atrophy was associated with lower baseline respiratory sinus arrhythmia (RSA; a  
75 parasympathetic measure) and skin conductance level (SCL; a sympathetic measure) in bvFTD.  
76 Next, we examined whether functional connectivity deficits in 21 autonomic-relevant, salience  
77 network node-pairs related to baseline autonomic dysfunction. Lower baseline RSA was  
78 associated with smaller volume in left ventral anterior insula (vAI), weaker connectivity between  
79 bilateral vAI and bilateral anterior cingulate cortex (ACC), and stronger connectivity between  
80 bilateral ACC and bilateral hypothalamus/amygdala. Lower baseline SCL, in contrast, was  
81 associated with smaller volume in inferior temporal gyrus, dorsal mid-insula, and hypothalamus;  
82 weaker connectivity between bilateral ACC and right hypothalamus/amygdala; and stronger  
83 connectivity between bilateral dorsal anterior insula and periaqueductal gray. Our results suggest  
84 that baseline parasympathetic and sympathetic tone depend on the integrity of lateralized  
85 salience network hubs (left vAI for parasympathetic and right hypothalamus/amygdala for  
86 sympathetic) and highly calibrated ipsilateral and contralateral network connections. In bvFTD,  
87 deficits in this system may underlie resting parasympathetic and sympathetic disruption.

88

## AUTONOMIC NETWORK ARCHITECTURE

89 Significance Statement

90 The salience network maintains homeostasis and regulates autonomic nervous system activity.  
91 Whether within-network connectivity patterns underlie individual differences in resting  
92 parasympathetic and sympathetic nervous system activity, however, is not well understood. We  
93 measured baseline autonomic nervous system activity in healthy controls and patients with  
94 behavioral variant frontotemporal dementia, a neurodegenerative disease characterized by resting  
95 autonomic deficits, and probed how salience network dysfunction relates to diminished  
96 parasympathetic and sympathetic outflow. Our results indicate that baseline parasympathetic and  
97 sympathetic tone are the product of complex, opposing intra-network nodal interactions and  
98 depend on the integrity of highly tuned, lateralized salience network hubs (i.e., left ventral  
99 anterior insula for parasympathetic activity and right hypothalamus/amygdala for sympathetic  
100 activity).

101

## 102 Introduction

103 The salience network is a distributed brain system that produces emotions and monitors  
104 the dynamic conditions of the body (Seeley et al., 2007). With hubs in ventral anterior insula  
105 (vAI) and anterior cingulate cortex (ACC) and tight connections with ventral striatum and central  
106 pattern generators including the hypothalamus, amygdala, and periaqueductal gray (PAG), the  
107 salience network participates in and may coordinate autonomic nervous system (ANS)  
108 regulation. During emotions, the salience network triggers visceromotor changes that disrupt  
109 quiescence and move an organism from rest to action. At rest, the salience network adjusts the  
110 internal milieu to meet current metabolic and motivational conditions (Benarroch, 1993;  
111 Carmichael and Price, 1995; Ongur and Price, 2000; Saper, 2002; Barbas et al., 2003a; Critchley,  
112 2005; Beissner et al., 2013; Critchley and Harrison, 2013). A continuous stream of sensory  
113 information travels from the spinal cord through the brainstem via the lamina I spinothalamic  
114 pathway and vagal afferents. This interoceptive information is then relayed to the dorsal  
115 posterior insula, mid-insula, and onward to vAI, a physiological integration site that is thought to  
116 represent internal feeling states that color subjective emotional experience and shape behavior  
117 (Craig, 2002; Critchley, 2004; Craig, 2009; Damasio and Carvalho, 2013).

118 The salience network influences both the sympathetic and parasympathetic branches of  
119 the ANS. The sympathetic ANS (SANS) responds to arousing or threatening stimuli and  
120 mobilizes behavior (Saper, 2002). The parasympathetic ANS (PANS), in contrast, downregulates  
121 arousal via the inhibitory influence of the vagus nerve. The vagus sends efferent signals from the  
122 brain to the internal organs, reducing heart rate to a pace that is slower than that set by the  
123 sinoatrial node (Carlson et al., 1992; Levy et al., 1993; Saper, 2002; Thayer and Siegle, 2002)  
124 and creating a “rest and digest” state that fosters interpersonal engagement and emotional

## AUTONOMIC NETWORK ARCHITECTURE

125 attunement (Porges, 2001). These two ANS branches appear to be asymmetrically organized in  
 126 the brain. While right-lateralized (i.e., non-dominant hemisphere) neural pathways promote  
 127 SANS outflow, left-lateralized (i.e., dominant hemisphere) systems facilitate PANS activity  
 128 (Oppenheimer et al., 1992; Oppenheimer et al., 1996; Yoon et al., 1997; Wittling et al., 1998a;  
 129 Wittling et al., 1998b; Craig, 2005; Guo et al., 2016).

130 Although previous research has examined how salience network connectivity relates to  
 131 PANS activity (Guo et al., 2016), it remains unknown how within-network nodal interactions  
 132 relate to individual differences in resting PANS and SANS function. The behavioral variant of  
 133 frontotemporal dementia (bvFTD) is a neurodegenerative disease that targets the salience  
 134 network (Seeley et al., 2007; Zhou et al., 2010) and offers a unique opportunity to examine how  
 135 salience network integrity relates to ANS deficits. In bvFTD there is progressive deterioration of  
 136 social behavior, empathy, and emotion (Rascovsky et al., 2007; Seeley et al., 2008; Kumfor and  
 137 Piguet, 2012; Seeley et al., 2012; Barsuglia et al., 2014; Joshi et al., 2014b; Levenson et al.,  
 138 2014; Mendez et al., 2014). In addition to deficits in emotion generation (Sturm et al., 2006;  
 139 Sturm et al., 2008; Eckart et al., 2012), patients with bvFTD also exhibit PANS and SANS  
 140 deficits at rest (Joshi et al., 2014a; Guo et al., 2016).

141 In the present study, we investigated whether specific patterns of salience network  
 142 dysfunction related to resting PANS and SANS deficits. We measured baseline ANS activity in  
 143 patients with bvFTD and healthy controls (HC) during a laboratory-based testing session.  
 144 Participants also underwent structural magnetic resonance imaging (MRI) and task-free  
 145 functional MRI (fMRI). Building on previous studies (Benarroch, 1993; Thayer and Lane, 2000;  
 146 Craig, 2002; Saper, 2002; Seeley et al., 2012; Critchley and Harrison, 2013; Damasio and  
 147 Carvalho, 2013), we developed a neural systems model (Figure 1A) to guide our examination of

## AUTONOMIC NETWORK ARCHITECTURE

148 nodes and edges (i.e., connectivity between node-pairs) that are embedded in the salience  
 149 network and support ANS activity. We hypothesized that lateralized network impairment would  
 150 be associated with resting ANS deficits such that left-sided dysfunction would predict  
 151 diminished PANS activity whereas right-sided dysfunction would predict lower SANS activity.

## 152 Materials and Methods

### 153 *Participants*

154 We included 47 participants in the present study: 24 HC (56.7 – 79.6 years of age) and 23  
 155 patients with bvFTD (34.2 – 71.2 years of age) (Rascovsky et al., 2007). The HC were recruited  
 156 from advertisements and were free of current or previous neurological or psychiatric disorders.  
 157 Patients underwent an interdisciplinary team evaluation at the University of California, San  
 158 Francisco (UCSF) Memory and Aging Center that included a clinical interview, neurological  
 159 exam, functional assessment, MRI, and neuropsychological testing (Table 1). A functional  
 160 assessment of dementia severity was obtained using the Clinical Dementia Rating Scale (CDR)  
 161 (Morris, 1993). Body mass index (BMI) was calculated for all patients and for 20/21 of HC with  
 162 available height and weight data. Participants were not taking medications at the time of the  
 163 laboratory assessment (described below) that could significantly affect ANS functioning (i.e.,  
 164 stimulants, beta-blockers, or acetylcholinesterase inhibitors). Power calculations based on  
 165 previous studies of ANS dysfunction in bvFTD (Joshi et al., 2014a; Guo et al., 2016) showed  
 166 that an  $\alpha = .05$  level test in a sample of this size had power greater than 80% to detect a difference  
 167 between the groups.

### 168 *Experimental Design and Statistical Analysis*

#### 169 *Laboratory Assessment of Autonomic Physiology*



170       *Procedure.* After informed consent, participants' physiological functioning was assessed  
 171 at the Berkeley Psychophysiology Laboratory at the University of California, Berkeley  
 172 (Levenson et al., 2008).

173       *Resting Baseline Autonomic Physiology.* Eleven 35-second resting baseline periods were  
 174 extracted from a task in which participants viewed 11 short films; for complete details, see  
 175 previous task descriptions (Goodkind et al., 2015). During these pre-film baseline periods,  
 176 participants were instructed to relax and to watch an "X" on a white monitor screen.

177       *Measures.* Physiological measures were monitored continuously using a Grass Model 7  
 178 or Biopac polygraph, a computer with analog-to-digital capability, and an online data acquisition  
 179 and analysis software package written by Robert W. Levenson. The software computed second-  
 180 by-second averages for the following measures: (1) heart rate (Beckman miniature electrodes  
 181 with Redux paste were placed in a bipolar configuration on opposite sides of the participant's  
 182 chest; the inter-beat interval was calculated as the interval, in milliseconds, between successive R  
 183 waves); (2) respiratory sinus arrhythmia (RSA), the peak-valley method was used, which  
 184 measures the time differences between the shortest inter-beat interval during inspiration and the  
 185 longest inter-beat interval during expiration on each breath (Grossman et al., 1990); (3) skin  
 186 conductance level (SCL), a constant-voltage device was used to pass a small voltage between  
 187 Beckman regular electrodes (using an electrolyte of sodium chloride in Unibase) attached to the  
 188 palmar surface of the middle phalanges of the ring and index fingers of the non-dominant hand;  
 189 (4) respiration period (a pneumatic bellows was stretched around the thoracic region and the  
 190 inter-cycle interval was measured in milliseconds between successive inspirations); and (5)  
 191 finger temperature (a thermistor attached to the distal phalanx of the little finger of the non-  
 192 dominant hand recorded temperature in degrees Fahrenheit).

## AUTONOMIC NETWORK ARCHITECTURE

193 This array of measures was selected to sample from major ANS (cardiovascular,  
 194 electrodermal, and respiratory) systems and enabled us to examine both PANS and SANS  
 195 integrity. RSA is a measure of vagally-mediated, beat-to-beat variation in heart rate, an index of  
 196 PANS activity (Berntson et al., 1997). RSA is closely linked to respiration, with heart rate  
 197 decelerating during expiration and accelerating during inspiration. We used the peak-valley  
 198 method, which quantifies the difference between the longest heart period during expiration and  
 199 the shortest heart period during inspiration (Grossman et al., 1990; Grossman and Taylor, 2007).  
 200 The natural logarithm of RSA (lnRSA) was used to improve proximity to a normal distribution  
 201 and was used in all analyses. SCL, which increases as there is greater innervation of the eccrine  
 202 sweat glands, is a relatively pure SANS measure (Critchley, 2002). Heart rate, respiration period,  
 203 and temperature are influenced by both ANS branches and, therefore, were not the focus of our  
 204 neuroimaging analyses.

205 Mean levels of physiological responding were computed for each 33-second pre-film  
 206 baseline (one second at the beginning and end of each baseline and trial were omitted to account  
 207 for measurement error in the timing of trial onset and offset) and were then averaged across all  
 208 11 baseline trials. We calculated a Cronbach's alpha reliability coefficient for each channel and  
 209 found high reliability for each measure across the 11 baseline periods (inter-beat interval=.99,  
 210 RSA=.94, SCL=.99, respiration period=.92, and temperature=.99), which suggests that the  
 211 overall baseline means were an accurate reflection of stable, trait-like baseline ANS physiology.

212 *Image Acquisition*

213 *Structural Imaging.* The majority of participants (17 HC and 22 patients) underwent  
 214 research-quality MRI within close proximity of the laboratory assessment of autonomic

## AUTONOMIC NETWORK ARCHITECTURE

215 physiology (4 months for patients and 12 months for HC). Structural images were obtained on a  
 216 3.0 Tesla Siemens (Siemens, Iselin, NJ) TIM Trio scanner equipped with a 12-channel head coil  
 217 located at the UCSF Neuroscience Imaging Center. Whole brain images were acquired using  
 218 volumetric MPRAGE (acquisition time=8:53, sagittal orientation, a field of view of 160 x 240 x  
 219 256 mm with an isotropic voxel resolution of 1 mm<sup>3</sup>, TR=2300 ms, TE=2.98 ms, TI=900 ms, flip  
 220 angle=9°).

221 *Functional Imaging.* Task-free fMRI scans were also obtained in 14 HC and 17 patients  
 222 with bvFTD. The 3T scanner acquired 240 task-free T2\*-weighted echoplanar fMRI volumes  
 223 (acquisition time=8:06, axial orientation with interleaved ordering, field of view=230 x 230 x  
 224 129 mm, matrix size=92 x 92, effective voxel resolution=2.5 x 2.5 x 3.0 mm, TR=2000 ms,  
 225 TE=27 ms)

226 *Image Preprocessing*

227 *Structural Imaging.* Structural T1 images were visually inspected for movement artifacts  
 228 before being processed with SPM12 (<http://www.fil.ion.ucl.ac.uk/spm/software/spm12/>). One  
 229 patient was excluded due to poor scan quality, leaving a total of 21 bvFTD and 17 HC. Within  
 230 the same generative model (Ashburner and Friston, 2005), the T1-weighted images were  
 231 segmented into gray and white matter using the segment program in SPM12. To guarantee  
 232 voxel-wise comparability, gray matter images were normalized to Montreal Neurological  
 233 Institute (MNI) space by applying 12-parameter linear transformation and non-linear warping,  
 234 modulated, and smoothed with an 8 mm full-width at half-maximum Gaussian kernel.

235 *Functional Imaging.* For each fMRI scan, the first five volumes were discarded. SPM12  
 236 and FSL (<http://fsl.fmrib.ox.ac.uk/fsl>) software were used for subsequent fMRI preprocessing.

## AUTONOMIC NETWORK ARCHITECTURE

237 The remaining 235 volumes were slice-time corrected, realigned to the mean functional image,  
 238 and assessed for rotational and translational head motion. Volumes were next co-registered to the  
 239 MP-RAGE image and then normalized to the standard MNI-152 healthy adult brain template  
 240 using SPM segment, producing MNI-registered volumes with 2 mm<sup>3</sup> isotropic resolution. These  
 241 volumes were spatially smoothed with a 6 mm radius Gaussian kernel and temporally bandpass  
 242 filtered in the .008-.15 Hz frequency range using fslmaths. Nuisance parameters in the  
 243 preprocessed data were estimated for the cerebrospinal fluid (CSF) using a mask in the central  
 244 portion of the lateral ventricles and for the white matter (WM) using a mask of the highest  
 245 probability cortical WM as labeled in the FSL tissue prior mask. Additional nuisance parameters  
 246 included the 3 translational and 3 rotational motion parameters, the temporal derivatives of the  
 247 previous 8 terms (WM/CSF/6 motion), and the squares of the previous 16 terms (Satterthwaite et  
 248 al., 2013). Any participant with a maximum relative head translation greater than 3 mm,  
 249 maximum relative rotation greater than 3 degrees, or more than 10% of frames with a motion  
 250 spike greater than 1 mm, were excluded from the analysis. Previous work has shown that the  
 251 edges tested in the present study have moderate to good test-retest reliability with this level of  
 252 head movement excluded (Guo et al., 2012) and that resting state measures are reliable when  
 253 these preprocessing strategies are employed (Varikuti et al., 2017). We excluded two patients for  
 254 excessive motion, leaving 14 HC and 15 patients with bvFTD. The groups (controlling for age,  
 255 sex, and education) did not significantly differ on total head movement during the scan,  $F(1,$   
 256  $24)=1.43, p=.24, \eta_p^2=.06$ .

### 257 *Analyses*

258 *Structural Neuroimaging Analyses.* We conducted separate whole-brain voxel-based  
 259 morphometry (VBM) analyses (Bates et al., 2003) in the patients to identify brain regions in

260 which smaller gray matter volume was associated with baseline RSA and SCL deficits in bvFTD  
 261 (Table 2). We chose to run the structural neuroimaging analyses in the patients only because they  
 262 have significantly more atrophy than the controls in many of the regions that we expected would  
 263 be related to the ANS measures and, thus, might unduly bias the analyses if we combined all of  
 264 the participants. Age, sex, education were included as nuisance covariates. In a follow-up  
 265 analysis, we added SCL as an additional covariate in the RSA analysis and RSA as an additional  
 266 covariate in the SCL analysis, which further allowed us to examine the independence of the  
 267 neural correlates of each measure. A priori significance was established at uncorrected  $p < .001$ .  
 268 One thousand permutation analyses using combined peak and extent thresholds were run to  
 269 derive a study-specific error distribution to determine the one-tailed  $T$ -threshold at  $p_{FWE} < .05$ ,  
 270 corrected for multiple comparisons (Nichols and Holmes, 2002).

271 *Functional Connectivity Neuroimaging Analyses.* Using a graph theoretical framework,  
 272 we identified “connectivity clusters” that corresponded to the regions of interest (ROIs) in our  
 273 model (Figure 1B). The clusters were obtained from task-free fMRI data in an independent  
 274 cohort of 40 healthy older controls (20 males, all less than 66 years old) as previously described  
 275 (Guo et al., 2012). In brief, we used four vAI and dorsal anterior insula (dAI) seeds, drawn from  
 276 a meta-analysis of task-based fMRI studies that activated the insula (Kurth et al., 2010) to derive  
 277 four connectivity maps. These four maps were entered into a full-factorial analysis, which  
 278 identified brain regions with connectivity to the dAI clusters, to the vAI clusters, or to both the  
 279 dAI and vAI clusters. We extracted the blood-oxygen-level dependent (BOLD) time series from  
 280 21 clusters that corresponded to the ROIs in our *a priori* theoretical model (Figure 1A) and  
 281 created a matrix that consisted of the connectivity strength of the edges in that model. Because  
 282 the clusters are data-driven and have connectivity-based contours, they may sample a more

283 homogeneous functional signal and be better suited for matrix-based analyses than typical  
284 spherical or landmark-based ROIs (Shirer et al., 2012).

285 We used previously established methods (Sturm et al., 2013) to identify key edges  
286 associated with RSA and SCL. First, edges weights were *r*-to-*z* transformed, and we then ran  
287 correlation analyses across the patients and controls between RSA and the connectivity strength  
288 of all 210 edges in our matrix. We planned to include any regions for which the correlation  
289 coefficient was greater than or equal to .20, a small to medium effect size (Cohen, 1992) and a  
290 permissive inclusion threshold, as additional candidate predictor variables in subsequent  
291 regression analyses. Next, we ran hierarchical regression analyses in order to determine which  
292 edges were significant predictors of RSA, a conservative test of our hypotheses because edges  
293 must emerge as significant predictors from a group of candidate predictor regions. In step one,  
294 we entered age, sex, education, and diagnosis into the model. In step two, we used a “forward”  
295 entry model to determine which edges accounted for a significant amount of variance above and  
296 beyond the control variables; thus, edges that did not account for significant variance were  
297 excluded from the model. In this second step, we included as predictor candidates all of the  
298 edges that passed the .2 inclusion threshold from our correlation analyses. We ran three separate  
299 regression analyses for ipsilateral left-hemisphere edges, ipsilateral right-hemisphere edges, and  
300 edges that crossed to the contralateral hemisphere (i.e., left to right or right to left) to minimize  
301 potential collinearity between homologous regions. We also examined our models to confirm  
302 that there was only weak multicollinearity among variables (variance inflation factor<4). We  
303 next repeated this entire process to identify edges that were significant predictors of baseline  
304 SCL. For each regression, we visually inspected the histogram and P-P plot of the standardized  
305 residuals to ensure that the error terms were normally distributed. The plots showed that the

## AUTONOMIC NETWORK ARCHITECTURE

306 points generally followed the normal (diagonal) line with no outliers or strong deviations,  
307 indicating that the assumptions of the regression models were met.

308 To ensure that any associations between functional connectivity and ANS physiology  
309 were not due to atrophy, we conducted another set of hierarchical regression analyses for RSA  
310 and SCL. From the structural scans, we extracted the total gray matter volume from each ROI.  
311 Here, in addition to the other nuisance covariates (age, sex, education, and diagnosis), we also  
312 included the mean ROI volumes for each of the edges (i.e., the mean volume of each node that  
313 comprised the relevant edges) that had entered the original forward-entry regression models in  
314 step one. In step two, we included the connectivity strength of the edges that had entered the  
315 models in our original analyses.

316 We anticipated that any associations that we detected between ANS activity and  
317 functional connectivity would reflect a general relationship that is not specific to either  
318 diagnosis. To confirm that this was the case, we repeated the final regression models (for  
319 ipsilateral left-hemisphere edges, ipsilateral right-hemisphere edges, and edges that crossed to  
320 the contralateral hemisphere) for RSA and SCL in each diagnosis separately. Here, we included  
321 age, sex, and education as nuisance covariates in step one. In step two, we entered the edges that  
322 had explained a significant portion of the variance in the forward-entry regression models we had  
323 conducted across the sample. Although each diagnostic group was much smaller than the total  
324 sample and, thus, our power was substantially reduced in these analyses, our aim was to  
325 investigate whether the effect sizes of any the associations between functional connectivity and  
326 ANS activity that we detected across the sample were comparable in each of the diagnostic  
327 groups when examined separately.

328 In a separate set of regressions, we examined whether the mean connectivity strength of  
 329 the edges that entered the regression RSA and SCL models were lower in bvFTD compared to  
 330 HC. In these analyses, the independent variable was diagnosis (bvFTD or HC), and the  
 331 covariates included age, sex, and years of education.

### 332 Results

333 *Smaller left vAI volume and lower vAI – ACC connectivity are associated with lower baseline*  
 334 *PANS activity*

335 In bvFTD, lower RSA was related to atrophy in a large cluster within left vAI, among  
 336 other regions (Table 3 and Figure 2A). When we also controlled for SCL in this RSA analysis,  
 337 the results remained largely unchanged though some regions that were more weakly associated  
 338 with RSA no longer remained significant (Table 3 and Figure 2B). Forward-entry hierarchical  
 339 regression analyses across the bvFTD and HC groups determined that weaker functional  
 340 connectivity in bilateral vAI – ACC edges, including left vAI – left ACC (2–5), left vAI – right  
 341 ACC (2–16), and right vAI – right ACC (13–15), was associated with lower baseline RSA  
 342 (Table 4 and Figure 2C). The functional connectivity results remained significant after atrophy  
 343 correction. When we repeated the original regression analyses in each diagnosis separately, there  
 344 were similar associations between RSA and the functional connectivity measures (Figure 4-1).  
 345 Patients with bvFTD had significantly lower connectivity strength than the HC in the right vAI –  
 346 right ACC (13–15) and left ACC – right amygdala (6–18) edges (Table 5). These findings  
 347 indicate that structural and functional deterioration of vAI (left > right) and its connections with  
 348 ACC are associated with a loss of basal parasympathetic tone as measured by RSA.



349 *Stronger connectivity in ACC – hypothalamus/amygdala edges relates to lower baseline PANS*  
 350 *activity*

351 Although lower RSA was associated with weaker vAI – ACC connectivity, the regression  
 352 analyses also revealed that lower RSA was associated with stronger connectivity in other edges.  
 353 Most notably, stronger connections between bilateral ACC and predominantly right-sided  
 354 hypothalamus/amygdala edges were associated with lower RSA (Table 4 and Figure 2C). This  
 355 pattern was not mirrored in the VBM analyses in that there were no regions where larger volume  
 356 was associated with lower RSA. All of the functional connectivity results held with atrophy  
 357 correction, with the exception of the right pregenual ACC – right hypothalamus ( $p=.07$ ) and right  
 358 vAI – right hypothalamus ( $p=.30$ ) edges. These results suggest that RSA depends on both  
 359 functional integrity of vAI – ACC edges and suppressed connectivity in ACC – hypothalamus  
 360 and ACC – amygdala edges (particularly in the right hemisphere), regions that appear to inhibit  
 361 PANS activity, perhaps by promoting SANS outflow.

362 *Stronger connectivity in ACC – hypothalamus/amygdala edges relates to higher SANS activity*

363 If the hypothalamus and amygdala promote SANS activity as suggested by the RSA  
 364 analyses, then we would expect that preserved volume and connectivity in these regions would  
 365 be associated with higher SCL. Consistent with this framework, larger volume in left inferior  
 366 temporal gyrus and left hypothalamus as well as right hypothalamus, amygdala and  
 367 periaqueductal gray (at a more permissive threshold of  $p<.005$ ) was associated with higher SCL  
 368 (Table 3 and Figure 3A). Furthermore, when we also controlled for RSA in this SCL analysis,  
 369 the results remained largely unchanged though some regions that were more weakly associated  
 370 with SCL no longer remained significant (Table 3 and Figure 3B). Stronger bilateral ACC –

## AUTONOMIC NETWORK ARCHITECTURE

hypothalamus connectivity was also associated with higher baseline SCL (Table 4 and Figure 3C). Although there were no regions for which larger volume was associated with lower SCL, stronger connectivity in bilateral dAI – PAG and left anterior midcingulate cortex (aMCC) – right hypothalamus edges did relate to lower SCL (Table 4 and Figure 3C). All functional connectivity results held with atrophy correction. When we repeated the original regression analyses in each diagnosis separately, there were similar associations between SCL and the functional connectivity measures (Figure 4-1). Taken together, these findings suggest that the right hypothalamus in particular is a key hub in SANS outflow and that atrophy and diminished connectivity in right hypothalamus/amygdala edges impede SCL. Patients with bvFTD had significantly lower connectivity strength than the HC in the left ACC – right hypothalamus (6–19), right ACC – right amygdala (16–18), right ACC – left ACC (17–5), right dAI – PAG (11–21), and left aMCC – right hypothalamus (4–19) edges (Table 5). Visual inspection of the data confirmed that significant associations that emerged between the functional connectivity measures and ANS activity were not driven by group effects (Figure 4).

## Discussion

The salience network coordinates the parasympathetic and sympathetic branches of the ANS (Benarroch, 1993; Ongur and Price, 2000; Thayer and Lane, 2000; Saper, 2002; Seeley et al., 2007; Beissner et al., 2013; Critchley and Harrison, 2013). This system enables the brain to trigger changes in the periphery and to receive continuous feedback about the physiological conditions of the body (Craig, 2002; Seeley et al., 2012; Critchley and Harrison, 2013). Previous research has revealed cerebral hemispheric asymmetry in PANS and SANS neural systems organization (Oppenheimer et al., 1992; Craig, 2005). Whereas the left hemisphere is essential for PANS functioning (Wittling et al., 1998a; Guo et al., 2016), the right hemisphere plays a

# AUTONOMIC NETWORK ARCHITECTURE

dominant role in SANS activation (Yoon et al., 1997; Wittling et al., 1998b). In keeping with this anatomical framework, our results suggest that healthy PANS and SANS activities are the product of complex, opposing intra-network nodal interactions. We found that the structural and functional integrity of specific hubs that have been identified in prior studies—left vAI for PANS and right hypothalamus/amygdala for SANS (Xavier et al., 2013; Guo et al., 2016)—were critical for maintaining resting ANS outflow. Although the left vAI and right hypothalamus/amygdala hubs were lateralized and located in the predicted hemispheres, they had connections with ipsilateral and contralateral network nodes that were also integral for baseline ANS activity. While ipsilateral pathways may facilitate within-hemisphere generation of PANS or SANS activity, contralateral projections may foster communication between hemispheres and enable system-level integration of PANS and SANS information. A distributed, bilateral ANS network that is anchored by asymmetric hubs may provide an efficient physiological system in which opposing PANS and SANS influences remain in a dynamic equilibrium at rest but can generate emotional reactions when needed.

*RSA depends on strong vAI – ACC integrity and weak ACC – hypothalamus/amygdala connectivity*

Our analyses revealed a constellation of nodes and edges that were associated with resting RSA. Consistent with previous findings, vAI and pregenual ACC emerged as key hubs of PANS control (Oppenheimer et al., 1996; Gianaros et al., 2004; Thayer et al., 2012; Allen et al., 2015; Guo et al., 2016; Jennings et al., 2016). Left vAI volume was positively associated with RSA in the structural neuroimaging analyses, and stronger connectivity in left vAI edges was also associated with higher RSA. vAI and pregenual ACC have tight reciprocal connections (Mesulam and Mufson, 1982; Carmichael and Price, 1996) and send projections to ANS

## AUTONOMIC NETWORK ARCHITECTURE

417 brainstem nuclei including the nucleus ambiguus and dorsal motor nucleus of the vagus (Shipley,  
418 1982; Hurley et al., 1991), a system that may promote the relay of PANS commands from  
419 cortical and subcortical hubs to peripheral organs such as the heart (Gatti et al., 1996).

420 In addition to edges in which stronger connectivity was associated with higher RSA,  
421 patients with weaker ACC – hypothalamus and ACC – amygdala connectivity had higher RSA.  
422 Interestingly, stronger connectivity in ACC – hypothalamus and ACC – amygdala edges was  
423 also associated with higher SCL, suggesting that the hypothalamus and amygdala (particularly in  
424 the right hemisphere) are central pattern generators essential for SANS outflow (Barbas and De  
425 Olmos, 1990; Laine et al., 2009; Xavier et al., 2013). Direct connections from ACC to the  
426 intermediolateral cell column (Bacon and Smith, 1993), or indirect connections through  
427 hypothalamus or amygdala (Saper et al., 1976; ter Horst et al., 1984; Barbas et al., 2003b), may  
428 promote SANS outflow. Therefore, higher connectivity between these regions and ACC may  
429 impede PANS activity by stimulating SANS outflow, consistent with prior studies showing an  
430 antagonistic relation between PANS and SANS activity (Levy, 1990; Saku et al., 2014). Our  
431 results suggest that RSA depends not only on strong connectivity in vAI – ACC, which promotes  
432 vagal tone, but also on relatively weak, or suppressed, connectivity in ACC –  
433 hypothalamus/amygdala, connections that encourage sympathetic outflow.

434 *SCL depends on ACC – hypothalamus/amygdala integrity and weak dAI – PAG connectivity*

435 Together with ACC, the amygdala and hypothalamus are integral SANS hubs (Bandler  
436 and Carrive, 1988; An et al., 1998; Ongur et al., 1998; Price, 1999; Ongur and Price, 2000). Our  
437 results indicate that stronger pregenua ACC – hypothalamus/amygdala connectivity was  
438 associated with higher SCL. Larger volume in inferior temporal gyrus, hypothalamus, amygdala,

## AUTONOMIC NETWORK ARCHITECTURE

439 and periaqueductal gray, among other regions, also predicted greater SCL activity. The integrity  
 440 of pregenual ACC and its direct projections with hypothalamus and amygdala, therefore, appears  
 441 to be essential for SANS outflow (Barbas and De Olmos, 1990; Davis and Whalen, 2001;  
 442 Ghashghaei and Barbas, 2002; Laine et al., 2009).

443 Like RSA, SCL depended on stronger connectivity in some edges but weaker  
 444 connectivity in others. Lower bilateral dAI – PAG and left aMCC – right hypothalamus  
 445 connectivity was associated with higher SANS tone. Both aMCC and dAI are key structures in  
 446 an inhibitory control system that constrains cognition and behavior and may also downregulate  
 447 physiological arousal (Aron et al., 2004; Nee et al., 2007; Touroutoglou et al., 2012; Enriquez-  
 448 Geppert et al., 2013; Hoffstaedter et al., 2014). Through connections with lateral frontoparietal  
 449 task control networks (Mesulam and Mufson, 1982; Mufson and Mesulam, 1982), dAI plays a  
 450 central role in response inhibition and emotion suppression (Aron, 2007; Giuliani et al., 2011).  
 451 The structural and functional integrity of aMCC has been associated with greater heart rate  
 452 variability (Critchley et al., 2003; Winkelmann et al., 2016), and connectivity in this region,  
 453 therefore, may contribute to dampening, rather than inducing physiological arousal. Although we  
 454 were unable to examine substructures within our subcortical ROIs, this hypothesis would be  
 455 especially compelling if the connectivity strength from our PAG and hypothalamus ROIs  
 456 primarily captured the activity of their PANS-relevant subregions (Bandler and Shipley, 1994; da  
 457 Silva et al., 2003) (Figure 5). Weakened connectivity in a PANS-mediated visceromotor braking  
 458 system, therefore, may facilitate SANS activity. In bvFTD, atrophy and connectivity disruption  
 459 involving both PANS and SANS structures likely resulted in a net loss of RSA and SCL activity  
 460 despite altered intra-network nodal interactions.

*Limitations*

462        There are several limitations of the present study that should be considered. First, the HC  
463        were older than the patients with bvFTD. Given that RSA and SCL decline in normal aging  
464        (Barontini et al., 1997; Masi et al., 2007), the age distribution of our sample would work against  
465        our hypothesis and make it more difficult for us to detect ANS impairment in the younger  
466        clinical group. Furthermore, we took several additional steps to mitigate the potential impact of  
467        age on our results: (1) our primary analyses were regression analyses rather than group  
468        comparisons, which allowed us to investigate how brain volume and functional connectivity  
469        related to ANS activity across the diagnostic groups, (2) we included age as a covariate in all  
470        analyses, (3) we conducted a follow-up analysis on ANS activity in a subgroup of patients who  
471        were age-matched and continued to find PANS and SANS deficits in bvFTD, a pattern that is  
472        consistent with previous studies (Joshi et al., 2014a; Guo et al., 2016). We also found that  
473        patients had faster baseline respiration rates, an alteration that may also reflect disruption of  
474        vagal pathways (Carlson et al., 1992; Critchley, 2002; Rybak et al., 2004). Given that our sample  
475        size was relatively small, additional studies are needed to detect the more subtle relationships  
476        that might exist between functional connectivity and ANS outflow. Larger studies of bvFTD will  
477        also be critical for elucidating whether RSA deficits relate to the alterations in respiration that we  
478        detected. Second, our study was not able to examine the functional connectivity of many relevant  
479        ANS brainstem nuclei, and many of our subcortical ROIs could have been deconstructed further  
480        into anatomically meaningful subregions with specific PANS and SANS roles. The  
481        hypothalamus and PAG, for example, can be divided into subregions that receive distinct  
482        projections from ACC and vAI and play different roles in PANS and SANS (Bandler and  
483        Shipley, 1994; Price, 1999). Because of this limitation, we may have failed to detect important  
484        associations between these subregions and our ANS measures. Future studies that are able to

## AUTONOMIC NETWORK ARCHITECTURE

485 subdivide these small structures into even finer parcels will continue to elucidate the neural  
486 architecture of ANS functioning. Third, whereas our PANS measure, RSA, was a cardiovascular  
487 measure, our SANS measure, SCL, was an electrodermal measure. Future studies that utilize  
488 cardiovascular measures of SANS activity, such as impedance cardiography, could help to  
489 determine whether all aspects of SANS activity are similarly disrupted in bvFTD or whether the  
490 SANS impairment is specific to electrodermal outflow. Given that SCL is a cholinergic, rather  
491 than an adrenergic, SANS measure, it is also possible that cholinergic dysfunction in bvFTD may  
492 underlie both the RSA and SCL deficits that we detected. Whether the adrenergic system is also  
493 altered in bvFTD will need to be addressed in future studies.

494 *Conclusion*

495 Although a single distributed neural network supports ANS physiology, opposing PANS  
496 and SANS subsystems within this network play distinct roles in homeostasis maintenance. Our  
497 results suggest that highly calibrated connections within the PANS and SANS subnetworks  
498 promote ANS outflow. Disruption of these subsystems in bvFTD may tip the autonomic balance  
499 and alter resting physiology as well as emotional responding. These findings may have wider  
500 implications for the study of psychiatric conditions with alterations in emotion and behavior.

## References

- 501  
502 Allen B, Jennings JR, Gianaros PJ, Thayer JF, Manuck SB (2015) Resting high-frequency heart  
503 rate variability is related to resting brain perfusion. *Psychophysiology* 52:277-287.
- 504 An X, Bandler R, Ongur D, Price JL (1998) Prefrontal cortical projections to longitudinal  
505 columns in the midbrain periaqueductal gray in macaque monkeys. *J Comp Neurol*  
506 401:455-479.
- 507 Aron AR (2007) The neural basis of inhibition in cognitive control. *The Neuroscientist* 13:214-  
508 228.
- 509 Aron AR, Robbins TW, Poldrack RA (2004) Inhibition and the right inferior frontal cortex.  
510 *Trends Cogn Sci* 8:170-177.
- 511 Ashburner J, Friston KJ (2005) Unified segmentation. *Neuroimage* 26:839-851.
- 512 Bacon SJ, Smith AD (1993) A monosynaptic pathway from an identified vasomotor centre in the  
513 medial prefrontal cortex to an autonomic area in the thoracic spinal cord. *Neuroscience*  
514 54:719-728.
- 515 Bandler R, Carrive P (1988) Integrated defence reaction elicited by excitatory amino acid  
516 microinjection in the midbrain periaqueductal grey region of the unrestrained cat. *Brain*  
517 Res 439:95-106.
- 518 Bandler R, Shipley MT (1994) Columnar organization in the midbrain periaqueductal gray:  
519 modules for emotional expression? *Trends Neurosci* 17:379-389.
- 520 Barbas H, De Olmos J (1990) Projections from the amygdala to basoventral and mediodorsal  
521 prefrontal regions in the rhesus monkey. *J Comp Neurol* 300:549-571.
- 522 Barbas H, Saha S, Rempel-Clower N, Ghashghaei T (2003a) Serial pathways from primate  
523 prefrontal cortex to autonomic areas may influence emotional expression. *BMC*  
524 *Neurosci* 10:25.



## AUTONOMIC NETWORK ARCHITECTURE

- 525 Barbas H, Saha S, Rempel-Clower N, Ghashghaei T (2003b) Serial pathways from primate  
526 prefrontal cortex to autonomic areas may influence emotional expression. *BMC Neurosci*  
527 4:25.
- 528 Barontini M, Lazzari JO, Levin G, Armando I, Basso SJ (1997) Age-related changes in  
529 sympathetic activity: biochemical measurements and target organ responses. *Arch*  
530 *Gerontol Geriatr* 25:175-186.
- 531 Barsuglia JP, Kaiser NC, Wilkins SS, Joshi A, Barrows RJ, Paholpak P, Panchal HV, Jimenez  
532 EE, Mather MJ, Mendez MF (2014) A scale of socioemotional dysfunction in  
533 frontotemporal dementia. *Archives of clinical neuropsychology : the official journal of*  
534 *the National Academy of Neuropsychologists* 29:793-805.
- 535 Bates E, Wilson SM, Saygin AP, Dick F, Sereno MI, Knight RT, Dronkers NF (2003) Voxel-  
536 based lesion-symptom mapping. *Nat Neurosci* 6:448-450.
- 537 Beissner F, Meissner K, Bar KJ, Napadow V (2013) The autonomic brain: an activation  
538 likelihood estimation meta-analysis for central processing of autonomic function. *J*  
539 *Neurosci* 33:10503-10511.
- 540 Benarroch EE (1993) The central autonomic network: functional organization, dysfunction, and  
541 perspective. *Mayo Clin Proc* 68:988-1001.
- 542 Berntson GG, Bigger JT, Jr., Eckberg DL, Grossman P, Kaufmann PG, Malik M, Nagaraja HN,  
543 Porges SW, Saul JP, Stone PH, van der Molen MW (1997) Heart rate variability: origins,  
544 methods, and interpretive caveats. *Psychophysiology* 34:623-648.
- 545 Carlson MD, Geha AS, Hsu J, Martin PJ, Levy MN, Jacobs G, Waldo AL (1992) Selective  
546 stimulation of parasympathetic nerve fibers to the human sinoatrial node. *Circulation*  
547 85:1311-1317.

## AUTONOMIC NETWORK ARCHITECTURE

- 548 Carmichael ST, Price JL (1995) Limbic connections of the orbital and medial prefrontal cortex in  
549 macaque monkeys. *Journal of Comparative Neurology* 363:615-641.
- 550 Carmichael ST, Price JL (1996) Connectional networks within the orbital and medial prefrontal  
551 cortex of macaque monkeys. *J Comp Neurol* 371:179-207.
- 552 Cohen J (1992) A power primer. *Psychol Bull* 112:155-159.
- 553 Craig AD (2002) How do you feel? Interoception: The sense of the physiological condition of  
554 the body. *Nat Rev Neurosci* 3:655-666.
- 555 Craig AD (2005) Forebrain emotional asymmetry: A neuroanatomical basis? *Trends in Cognitive*  
556 *Science* 9:566-571.
- 557 Craig AD (2009) How do you feel--now? The anterior insula and human awareness. *Nat Rev*  
558 *Neurosci* 10:59-70.
- 559 Critchley HD (2002) Electrodermal responses: what happens in the brain. *Neuroscientist* 8:132-  
560 142.
- 561 Critchley HD (2004) The human cortex responds to an interoceptive challenge. *Proceedings of*  
562 *the National Academy of Sciences of the United States of America* 101:6333-6334.
- 563 Critchley HD (2005) Neural mechanisms of autonomic, affective, and cognitive integration. *The*  
564 *Journal of Comparative Neurology* 493:154-166.
- 565 Critchley HD, Harrison NA (2013) Visceral influences on brain and behavior. *Neuron* 77:624-  
566 638.
- 567 Critchley HD, Mathias CJ, Josephs O, O'Doherty J, Zanini S, Dewar BK, Cipolotti L, Shallice T,  
568 Dolan RJ (2003) Human cingulate cortex and autonomic control: Converging  
569 neuroimaging and clinical evidence. *Brain* 126:2139-2152.

## AUTONOMIC NETWORK ARCHITECTURE

- 570 da Silva LG, de Menezes RC, dos Santos RA, Campagnole-Santos MJ, Fontes MA (2003) Role  
 571 of periaqueductal gray on the cardiovascular response evoked by disinhibition of the  
 572 dorsomedial hypothalamus. *Brain Res* 984:206-214.
- 573 Damasio A, Carvalho GB (2013) The nature of feelings: evolutionary and neurobiological  
 574 origins. *Nat Rev Neurosci* 14:143-152.
- 575 Davis M, Whalen PJ (2001) The amygdala: Vigilance and emotion. *Molecular Psychiatry* 6:13-  
 576 34.
- 577 Eckart JA, Sturm VE, Miller BL, Levenson RW (2012) Diminished disgust reactivity in  
 578 behavioral variant frontotemporal dementia. *Neuropsychologia* 50:786-790.
- 579 Enriquez-Geppert S, Eichele T, Specht K, Kugel H, Pantev C, Huster RJ (2013) Functional  
 580 parcellation of the inferior frontal and midcingulate cortices in a flanker-stop-change  
 581 paradigm. *Hum Brain Mapp* 34:1501-1514.
- 582 Gatti PJ, Johnson TA, Massari VJ (1996) Can neurons in the nucleus ambiguus selectively  
 583 regulate cardiac rate and atrio-ventricular conduction? *J Auton Nerv Syst* 57:123-127.
- 584 Ghashghaei HT, Barbas H (2002) Pathways for emotion: interactions of prefrontal and anterior  
 585 temporal pathways in the amygdala of the rhesus monkey. *Neuroscience* 115:1261-1279.
- 586 Gianaros PJ, Van Der Veen FM, Jennings JR (2004) Regional cerebral blood flow correlates  
 587 with heart period and high-frequency heart period variability during working-memory  
 588 tasks: Implications for the cortical and subcortical regulation of cardiac autonomic  
 589 activity. *Psychophysiology* 41:521-530.
- 590 Giuliani NR, Drabant EM, Bhatnagar R, Gross JJ (2011) Emotion regulation and brain plasticity:  
 591 expressive suppression use predicts anterior insula volume. *Neuroimage* 58:10-15.

## AUTONOMIC NETWORK ARCHITECTURE

- 592 Goodkind MS, Sturm VE, Ascher EA, Shdo SM, Miller BL, Rankin KP, Levenson RW (2015)  
 593 Emotion recognition in frontotemporal dementia and Alzheimer's disease: A new film-  
 594 based assessment. *Emotion* 15:416-427.
- 595 Grossman P, Taylor EW (2007) Toward understanding respiratory sinus arrhythmia: relations to  
 596 cardiac vagal tone, evolution and biobehavioral functions. *Biol Psychol* 74:263-285.
- 597 Grossman P, van Beek J, Wientjes C (1990) A comparison of three quantification methods for  
 598 estimation of respiratory sinus arrhythmia. *Psychophysiology* 27:702-714.
- 599 Guo CC, Kurth F, Zhou J, Mayer EA, Eickhoff SB, Kramer JH, Seeley WW (2012) One-year  
 600 test-retest reliability of intrinsic connectivity network fMRI in older adults. *Neuroimage*  
 601 61:1471-1483.
- 602 Guo CC, Sturm VE, Zhou J, Gennatas ED, Trujillo AJ, Hua AY, Crawford R, Stables L, Kramer  
 603 JH, Rankin K, Levenson RW, Rosen HJ, Miller BL, Seeley WW (2016) Dominant  
 604 hemisphere lateralization of cortical parasympathetic control as revealed by  
 605 frontotemporal dementia. *Proc Natl Acad Sci U S A* 113:E2430-2439.
- 606 Hoffstaedter F, Grefkes C, Caspers S, Roski C, Palomero-Gallagher N, Laird AR, Fox PT,  
 607 Eickhoff SB (2014) The role of anterior midcingulate cortex in cognitive motor control:  
 608 evidence from functional connectivity analyses. *Hum Brain Mapp* 35:2741-2753.
- 609 Hurley KM, Herbert H, Moga MM, Saper CB (1991) Efferent projections of the infralimbic  
 610 cortex of the rat. *J Comp Neurol* 308:249-276.
- 611 Jennings JR, Sheu LK, Kuan DC, Manuck SB, Gianaros PJ (2016) Resting state connectivity of  
 612 the medial prefrontal cortex covaries with individual differences in high-frequency heart  
 613 rate variability. *Psychophysiology* 53:444-454.

## AUTONOMIC NETWORK ARCHITECTURE

- 614 Joshi A, Mendez MF, Kaiser N, Jimenez E, Mather M, Shapira JS (2014a) Skin conductance  
 615 levels may reflect emotional blunting in behavioral variant frontotemporal dementia. J  
 616 Neuropsychiatry Clin Neurosci 26:227-232.
- 617 Joshi A, Barsuglia JP, Mather MJ, Jimenez EE, Shapira J, Mendez MF (2014b) Evaluation of  
 618 emotional blunting in behavioral variant frontotemporal dementia compared to  
 619 Alzheimer's disease. Dement Geriatr Cogn Disord 38:79-88.
- 620 Kumfor F, Piguet O (2012) Disturbance of emotion processing in frontotemporal dementia: a  
 621 synthesis of cognitive and neuroimaging findings. Neuropsychol Rev 22:280-297.
- 622 Kurth F, Zilles K, Fox PT, Laird AR, Eickhoff SB (2010) A link between the systems: functional  
 623 differentiation and integration within the human insula revealed by meta-analysis. Brain  
 624 Structure and Function 214:519-534.
- 625 Laine CM, Spitler KM, Mosher CP, Gothard KM (2009) Behavioral triggers of skin conductance  
 626 responses and their neural correlates in the primate amygdala. J Neurophysiol 101:1749-  
 627 1754.
- 628 Levenson RW, Sturm VE, Haase CM (2014) Emotional and behavioral symptoms in  
 629 neurodegenerative disease: a model for studying the neural bases of psychopathology.  
 630 Annual review of clinical psychology 10:581-606.
- 631 Levenson RW, Ascher E, Goodkind M, McCarthy M, Sturm V, Werner K (2008) Chapter 25  
 632 Laboratory testing of emotion and frontal cortex. Handbook of clinical neurology 88:489-  
 633 498.
- 634 Levy MN (1990) Autonomic interactions in cardiac control. Ann N Y Acad Sci 601:209-221.

## AUTONOMIC NETWORK ARCHITECTURE

- 635 Levy MN, Yang T, Wallick DW (1993) Assessment of beat-by-beat control of heart rate by the  
 636 autonomic nervous system: molecular biology technique are necessary, but not sufficient.  
 637 J Cardiovasc Electrophysiol 4:183-193.
- 638 Masi CM, Hawkley LC, Rickett EM, Cacioppo JT (2007) Respiratory sinus arrhythmia and  
 639 diseases of aging: obesity, diabetes mellitus, and hypertension. Biol Psychol 74:212-223.
- 640 Mendez MF, Fong SS, Shapira JS, Jimenez EE, Kaiser NC, Kremen SA, Tsai PH (2014)  
 641 Observation of social behavior in frontotemporal dementia. Am J Alzheimers Dis Other  
 642 Demen 29:215-221.
- 643 Mesulam MM, Mufson EJ (1982) Insula of the old world monkey. I. Architectonics in the  
 644 insulo-orbito-temporal component of the paralimbic brain. Journal of Comparative  
 645 Neurology 212:1-22.
- 646 Morris JC (1993) The Clinical Dementia Rating (CDR): Current version and scoring rules.  
 647 Neurology 43:2412-2414.
- 648 Mufson EJ, Mesulam MM (1982) Insula of the old world monkey. II: Afferent cortical input and  
 649 comments on the claustrum. J Comp Neurol 212:23-37.
- 650 Nee DE, Wager TD, Jonides J (2007) Interference resolution: insights from a meta-analysis of  
 651 neuroimaging tasks. Cogn Affect Behav Neurosci 7:1-17.
- 652 Nichols TE, Holmes AP (2002) Nonparametric permutation tests for functional neuroimaging: a  
 653 primer with examples. Human Brain Mapping 15:1-25.
- 654 Ongur D, Price JL (2000) The organization of networks within the orbital and medial prefrontal  
 655 cortex of rats, monkeys, and humans. Cereb Cortex 10:206-219.
- 656 Ongur D, An X, Price JL (1998) Prefrontal cortical projections to the hypothalamus in macaque  
 657 monkeys. Journal of Comparative Neurology 401:480-505.

## AUTONOMIC NETWORK ARCHITECTURE

- 658 Oppenheimer SM, Kedem G, Martin WM (1996) Left-insular cortex lesions perturb cardiac  
 659 autonomic tone in humans. *Clinical Autonomic Research* 6:131-140.
- 660 Oppenheimer SM, Gelb A, Girvin JP, Hachinski VC (1992) Cardiovascular effects of human  
 661 insular cortex stimulation. *Neurology* 42:1727-1732.
- 662 Porges SW (2001) The polyvagal theory: phylogenetic substrates of a social nervous system.  
 663 *International journal of psychophysiology : official journal of the International*  
 664 *Organization of Psychophysiology* 42:123-146.
- 665 Price JL (1999) Prefrontal cortical networks related to visceral function and mood. *Ann N Y*  
 666 *Acad Sci* 877:383-396.
- 667 Rascovsky K, Hodges JR, Kipps CM, Johnson JK, Seeley WW, Mendez MF, Knopman D,  
 668 Kertesz A, Mesulam M, Salmon DP, Galasko D, Chow TW, Decarli C, Hillis A, Josephs  
 669 K, Kramer JH, Weintraub S, Grossman M, Gorno-Tempini ML, Miller BL (2007)  
 670 Diagnostic criteria for the behavioral variant of frontotemporal dementia (bvFTD):  
 671 Current limitations and future directions. *Alzheimer Disease and Associated Disorders*  
 672 21:S14-S18.
- 673 Rybak IA, Shevtsova NA, Paton JF, Dick TE, St-John WM, Morschel M, Dutschmann M (2004)  
 674 Modeling the ponto-medullary respiratory network. *Respiratory physiology &*  
 675 *neurobiology* 143:307-319.
- 676 Saku K, Kishi T, Sakamoto K, Hosokawa K, Sakamoto T, Murayama Y, Kakino T, Ikeda M, Ide  
 677 T, Sunagawa K (2014) Afferent vagal nerve stimulation resets baroreflex neural arc and  
 678 inhibits sympathetic nerve activity. *Physiological reports* 2.
- 679 Saper CB (2002) The central autonomic nervous system: Conscious visceral perception and  
 680 autonomic pattern generation. *Annual Review of Neuroscience* 25:433-469.

## AUTONOMIC NETWORK ARCHITECTURE

- 681 Saper CB, Loewy AD, Swanson LW, Cowan WM (1976) Direct hypothalamo-autonomic  
 682 connections. *Brain Res* 117:305-312.
- 683 Satterthwaite TD, Elliott MA, Gerraty RT, Ruparel K, Loughhead J, Calkins ME, Eickhoff SB,  
 684 Hakonarson H, Gur RC, Gur RE, Wolf DH (2013) An improved framework for confound  
 685 regression and filtering for control of motion artifact in the preprocessing of resting-state  
 686 functional connectivity data. *Neuroimage* 64:240-256.
- 687 Seeley WW, Zhou J, Kim EJ (2012) Frontotemporal dementia: What can the behavioral variant  
 688 teach us about human brain organization? *Neuroscientist* 18:373-385.
- 689 Seeley WW, Crawford R, Rascofsky K, Kramer JH, Weiner M, Miller BL, Gorno-Tempini ML  
 690 (2008) Frontal paralimbic network atrophy in very mild behavioral variant  
 691 frontotemporal dementia. *Arch Neurol* 65:249-255.
- 692 Seeley WW, Menon V, Schatzberg AF, Keller J, Glover GH, Kenna H, Reiss AL, Greicius MD  
 693 (2007) Dissociable intrinsic connectivity networks for salience processing and executive  
 694 control. *Journal of Neuroscience* 27:2349-2356.
- 695 Shipley MT (1982) Insular cortex projection to the nucleus of the solitary tract and brainstem  
 696 visceromotor regions in the mouse. *Brain Res Bull* 8:139-148.
- 697 Shirer WR, Ryali S, Rykhlevskaia E, Menon V, Greicius MD (2012) Decoding subject-driven  
 698 cognitive states with whole-brain connectivity patterns. *Cereb Cortex* 22:158-165.
- 699 Sturm VE, Ascher EA, Miller BL, Levenson RW (2008) Diminished self-conscious emotional  
 700 responding in frontotemporal lobar degeneration patients. *Emotion* 8:861-869.
- 701 Sturm VE, Allison SC, Rosen HJ, Miller BL, Levenson RW (2006) Self-conscious emotion  
 702 deficits in frontotemporal lobar degeneration. *Brain* 129:2508-2516.



## AUTONOMIC NETWORK ARCHITECTURE

- 703 Sturm VE, Sollberger M, Seeley WW, Rankin KP, Ascher EA, Rosen HJ, Miller BL, Levenson  
 704 RW (2013) Role of right pregenual anterior cingulate cortex in self-conscious emotional  
 705 reactivity. *Soc Cogn Affect Neurosci* 8:468-474.
- 706 ter Horst GJ, Luiten PG, Kuipers F (1984) Descending pathways from hypothalamus to dorsal  
 707 motor vagus and ambiguus nuclei in the rat. *J Auton Nerv Syst* 11:59-75.
- 708 Thayer JF, Lane RD (2000) A model of neurovisceral integration in emotion regulation and  
 709 dysregulation. *J Affect Disord* 61:201-216.
- 710 Thayer JF, Siegle GJ (2002) Neurovisceral integration in cardiac and emotional regulation. *IEEE*  
 711 *Eng Med Biol Mag* 21:24-29.
- 712 Thayer JF, Ahs F, Fredrikson M, Sollers JJ, 3rd, Wager TD (2012) A meta-analysis of heart rate  
 713 variability and neuroimaging studies: implications for heart rate variability as a marker of  
 714 stress and health. *Neurosci Biobehav Rev* 36:747-756.
- 715 Touroutoglou A, Hollenbeck M, Dickerson BC, Feldman Barrett L (2012) Dissociable large-  
 716 scale networks anchored in the right anterior insula subserve affective experience and  
 717 attention. *Neuroimage* 60:1947-1958.
- 718 Varikuti DP, Hoffstaedter F, Genon S, Schwender H, Reid AT, Eickhoff SB (2017) Resting-state  
 719 test-retest reliability of a priori defined canonical networks over different preprocessing  
 720 steps. *Brain Struct Funct* 222:1447-1468.
- 721 Winkelmann T, Thayer JF, Pohlack S, Nees F, Grimm O, Flor H (2016) Structural brain  
 722 correlates of heart rate variability in a healthy young adult population. *Brain Struct Funct*.
- 723 Wittling W, Block A, Genzel S, Schweiger E (1998a) Hemisphere asymmetry in  
 724 parasympathetic control of the heart. *Neuropsychologia* 36:461-468.

## AUTONOMIC NETWORK ARCHITECTURE

- 725 Wittling W, Block A, Schweiger E, Genzel S (1998b) Hemisphere asymmetry in sympathetic  
726 control of the human myocardium. *Brain Cogn* 38:17-35.
- 727 Xavier CH, Beig MI, Ianzer D, Fontes MA, Nalivaiko E (2013) Asymmetry in the control of  
728 cardiac performance by dorsomedial hypothalamus. *American journal of physiology*  
729 *Regulatory, integrative and comparative physiology* 304:R664-674.
- 730 Yoon BW, Morillo CA, Cechetto DF, Hachinski V (1997) Cerebral hemispheric lateralization in  
731 cardiac autonomic control. *Arch Neurol* 54:741-744.
- 732 Zhou J, Greicius MD, Gennatas ED, Growdon ME, Jang JY, Rabinovici GD, Kramer JH, Weiner  
733 M, Miller BL, Seeley WW (2010) Divergent network connectivity changes in  
734 behavioural variant frontotemporal dementia and Alzheimer's disease. *Brain* 133:1352-  
735 1367.
- 736

737

## Acknowledgments

738 The authors would like to thank the patients, healthy controls, and their families for participating  
739 in our research studies. This project was supported by grants from the NIH National Institute on  
740 Aging (P50AG023501, P01AG019724, R01AG052496, R01AG032306, R01AG057204,  
741 1K23AG040127, and 1K23AG045289), The Larry L. Hillblom Foundation (2013-A-029-SUP  
742 and 2005/2T), the John Douglas French Foundation, the Consortium for Frontotemporal  
743 Dementia Research, and the Tau Consortium.

744

745

Table 1

*Participant characteristics classified by diagnostic group.* Means (*M*) and standard deviations (*SD*) are listed for each group unless otherwise noted. Neuropsychological testing included assessment of verbal and visual episodic memory, executive function (e.g., set-shifting, working memory, and fluency), language, and visuospatial functioning. A total of 19/23 patients and 17/24 HC completed neuropsychological testing in close proximity (within 4 months for patients and 12 months for the HC) to the laboratory assessment. The CDR Total and Sum of the Boxes were computed for each participant with higher scores indicating greater impairment. bvFTD= behavioral variant frontotemporal dementia, BMI= Body Mass Index, CDR Total= Clinical Dementia Rating Total score, CDR-SB= Clinical Dementia Rating Sum of Boxes, HC= healthy controls, and MMSE= Mini-Mental State Examination. † The HC received the California Verbal Learning Test-II (16-word list) instead of the Short Form. Their performance on the 20-minute delay was also in the average range ( $M= 13.6$ ,  $SD= 2.1$ ). We used analysis of variance and chi-square tests, when appropriate, to examine group differences. Partial eta squared ( $\eta_p^2$ ) is provided as a measure of effect size.

|                            | <i>bvFTD</i><br><i>M(SD)</i> | <i>HC</i><br><i>M(SD)</i> | <i>p</i> | $\eta_p^2$ |
|----------------------------|------------------------------|---------------------------|----------|------------|
| N                          | 23                           | 24                        |          |            |
| Age                        | 58.4 (8.4)                   | 67.9 (5.4)                | <.001    | .31        |
| Sex: % Female              | 30.4                         | 54.2                      | .10      |            |
| Education                  | 15.7 (2.9)                   | 17.6 (2.3)                | .02      | .12        |
| Handedness: % Right-handed | 100.0                        | 91.7                      | .16      |            |
| BMI                        | 32.2 (29.1)                  | 25.8 (12.3)               | .37      | .02        |
| CDR Total                  | 1.2 (0.6)                    | 0.0 (0.0)                 | <.001    | .72        |

## AUTONOMIC NETWORK ARCHITECTURE

|  |             |             |       |     |
|--|-------------|-------------|-------|-----|
| CDR-SB   | 7.2 (2.8)   | 0.0 (0.0)   | <.001 | .77 |
| MMSE   | 23.9 (5.2)  | 29.6 (0.6)  | <.001 | .38 |
| California Verbal Learning Test-<br>Short Form 10-Minute Recall (/9) | 3.8 (2.3)   | †           |       |     |
| Benson Figure Copy 10-Minute<br>Recall (/17)                         | 6.8 (4.4)   | 11.4 (2.6)  | .001  | .29 |
| Modified Trails (correct lines per<br>minute)                        | 13.9 (13.0) | 39.6 (12.1) | <.001 | .53 |
| Modified Trails Errors   | 2.4 (2.4)   | 0.2 (0.4)   | .001  | .31 |
| Phonemic Fluency (# correct in 60<br>seconds)                        | 5.5 (3.8)   | 19.2 (4.3)  | <.001 | .76 |
| Semantic Fluency (# correct in 60<br>seconds)                        | 9.1 (4.7)   | 24.0 (5.3)  | <.001 | .70 |
| Design Fluency Correct (# correct in<br>60 seconds)                  | 4.8 (3.3)   | 11.8 (2.8)  | <.001 | .58 |
| Design Fluency Repetitions   | 7.3 (6.3)   | 1.8 (2.4)   | .001  | .26 |
| Digits Backward  | 3.2 (0.9)   | 6.0 (1.4)   | <.001 | .61 |
| Benson Figure Copy (/17)   | 13.8 (2.1)  | 15.3 (1.0)  | .015  | .16 |
| Calculations (/5)  | 3.3 (1.1)   | 4.9 (0.2)   | <.001 | .54 |
| Boston Naming Test Spontaneous<br>Correct (/15)                      | 11.8 (3.1)  | 14.6 (0.7)  | <.001 | .30 |
| Peabody Picture Vocabulary Test<br>(/16)                             | 13.7 (3.3)  | 15.7 (0.6)  | .025  | .15 |

761

762 Table 2

763 *Resting baseline physiological levels.* Analyses of covariance (controlling for age, sex, and  
 764 education) found that patients with bvFTD (n=22) had significantly lower respiratory sinus  
 765 arrhythmia, lower skin conductance level, and shorter respiration period than the healthy controls  
 766 (n=22). When we added additional covariates that might influence RSA (i.e., resting inter-beat  
 767 interval, resting respiration period, and body mass index) to the model (while also controlling for  
 768 education, sex, and age), patients continued to have lower RSA,  $F(1, 33)= 469, p=.038, \eta_p^2=.13$ .  
 769 For SCL, although including resting inter-beat interval, resting respiration period, and body mass  
 770 index as additional covariates caused the difference to fall to trend levels, the pattern of results  
 771 was in the expected direction, with patients having lower SCL than controls,  $F(1, 32)= 2.82, p<$   
 772  $.11, \eta_p^2=.08$ . To examine whether the results of the original model (controlling for age, sex, and  
 773 education) held in a smaller, age-matched sample, we removed patients under age 58 (n=6) and  
 774 healthy controls over age 70 (n=8). In this subset of participants (17 bvFTD and 15 HC), the  
 775 patients and controls did not differ in age,  $F(1,31)=3.2, p=.09, \eta_p^2=.09$ . In this smaller sample, the  
 776 group differences in baseline autonomic activity remained significant. Compared to healthy  
 777 controls, patients with bvFTD had lower RSA,  $F(1,27)=5.6, p=.03, \eta_p^2=.17$ , lower SCL,  
 778  $F(1,27)=4.2, p=.05, \eta_p^2=.14$ , and shorter respiration period,  $F(1,27)=8.1, p=.008, \eta_p^2=.23$ . Means  
 779 ( $M$ ) and standard deviations ( $SD$ ) are reported. Partial eta squared ( $\eta_p^2$ ) is provided as a measure  
 780 of effect size. \* indicates significant differences at  $p<.05$  in the first model described above.

---

| <i>bvFTD</i> | <i>Healthy</i>  |          |          |            |
|--------------|-----------------|----------|----------|------------|
| <i>M(SD)</i> | <i>Controls</i> |          |          |            |
|              | <i>M(SD)</i>    | <i>F</i> | <i>p</i> | $\eta_p^2$ |

---

AUTONOMIC NETWORK ARCHITECTURE

|                                    |                |                |      |      |     |
|------------------------------------|----------------|----------------|------|------|-----|
| Inter-beat interval (ms)           | 906.6 (156.74) | 981.9 (133.9)  | 0.3  | .57  | .01 |
| Respiratory sinus arrhythmia (ms)* | 39.1 (22.9)    | 62.9 (55.3)    | 10.0 | .003 | .20 |
| Skin conductance level (μmhos)*    | 2.0 (0.9)      | 2.9 (1.7)      | 4.6  | .037 | .10 |
| Respiration period (ms)*           | 4035.6 (915.5) | 4750.3 (946.6) | 9.4  | .004 | .19 |
| Finger temperature (°F)            | 80.7 (5.5)     | 80.5 (5.6)     | 0.0  | .97  | .00 |

781

782

Table 3

*Anatomical correlates of baseline PANS and SANS activity.* Whole-brain VBM analyses in patients with bvFTD (controlling for age, sex, and education) revealed that atrophy in many ANS network nodes was associated with lower baseline RSA (n=21) and SCL (n=20). Montreal Neurological Institute coordinates (x, y, z) given for maximum *T*-score for the cluster (cluster size > 150 mm<sup>3</sup>). Results are significant at  $p < .001$ , uncorrected. † denotes significance at  $p_{\text{FWE}} < .05$ . To identify the independent neural correlates of PANS and SANS activity, we conducted follow-up VBM analyses when controlling for the opposing autonomic measure (i.e., including SCL as an additional covariate in the RSA VBM analysis and SCL as an additional covariate in the RSA VBM analysis). \* denotes significance at  $p < .001$ , uncorrected, when also controlling for the opposing autonomic measure.

| <i>Anatomical Region</i>       | <i>Cluster Volume (mm<sup>3</sup>)</i> | <i>x</i> | <i>y</i> | <i>z</i> | <i>Maximum T-score</i> | <i>β</i> |
|--------------------------------|--|----------|----------|----------|------------------------|----------|
| RSA                            |  |          |          |          |                        |          |
| Left ventral anterior insula*  | 1312                                   | -41      | 12       | -15      | 5.41                   | .79      |
| Left inferior temporal lobe*   | 448                                    | -32      | 2        | -36      | 4.96                   | .59      |
| Right parahippocampal gyrus    | 320                                    | 15       | 11       | -30      | 4.50                   | .63      |
| Left parahippocampal gyrus*    | 168                                    | -14      | 8        | -26      | 4.28                   | .68      |
| SCL                            |  |          |          |          |                        |          |
| Left inferior temporal gyrus†* | 6120                                   | -51      | -21      | -27      | 6.57                   | .77      |
| Left temporal pole*            | 1528                                   | -33      | 9        | -50      | 5.02                   | .72      |
| Right fusiform gyrus*          | 1200                                   | 27       | -15      | -41      | 5.05                   | .69      |
| Left precentral gyrus          | 1160                                   | -41      | -18      | 59       | 4.31                   | .75      |
| Left dorsal mid-insula*        | 1088                                   | -36      | 14       | 15       | 7.08                   | .61      |
| Left orbitofrontal cortex*     | 1080                                   | -21      | 18       | -16      | 4.71                   | .65      |
| Left orbitofrontal cortex*     | 1080                                   | -18      | 47       | -21      | 5.34                   | .67      |
| Right orbitofrontal cortex*    | 912                                    | 26       | 21       | -11      | 5.16                   | .54      |
| Right frontal pole*            | 880                                    | 8        | 71       | 14       | 5.77                   | .81      |
| Right frontal pole             | 776                                    | -15      | 69       | -11      | 5.38                   | .67      |
| Left parahippocampal gyrus*    | 712                                    | -11      | -8       | -35      | 5.60                   | .79      |



AUTONOMIC NETWORK ARCHITECTURE

|                               |     |     |     |     |      |     |
|-------------------------------|-----|-----|-----|-----|------|-----|
| Right middle frontal gyrus*   | 672 | 50  | 14  | 51  | 6.20 | .89 |
| Left superior frontal gyrus   | 600 | -17 | 41  | 51  | 4.65 | .81 |
| Right postcentral gyrus       | 584 | 23  | -30 | 74  | 4.25 | .76 |
| Right precentral gyrus*       | 496 | 44  | -20 | 60  | 4.30 | .69 |
| Left precuneus                | 424 | -17 | -41 | 71  | 4.94 | .70 |
| Left frontal pole*            | 424 | -38 | 56  | 9   | 4.30 | .66 |
| Left hypothalamus             | 424 | -8  | -5  | -9  | 4.14 | .60 |
| Left fusiform gyrus           | 416 | -33 | -17 | -44 | 4.17 | .73 |
| Right gyrus rectus            | 352 | 9   | 33  | -17 | 4.16 | .54 |
| Right precentral gyrus        | 320 | 35  | -8  | 62  | 4.75 | .80 |
| Left fusiform gyrus           | 304 | 51  | -11 | -29 | 4.33 | .60 |
| Left inferior parietal lobe   | 280 | -47 | -50 | 54  | 4.29 | .73 |
| Right superior frontal gyrus* | 280 | 23  | 57  | 36  | 5.16 | .67 |
| Left precentral gyrus*        | 264 | -32 | -9  | 63  | 4.33 | .77 |
| Right cerebellum*             | 232 | 35  | -50 | -45 | 4.02 | .50 |
| Left pars triangularis        | 200 | -33 | 33  | 3   | 4.09 | .75 |
| Right inferior parietal lobe  | 192 | 48  | -42 | 59  | 4.38 | .66 |
| Left supplementary motor area | 160 | -9  | 8   | 65  | 4.61 | .63 |

794

795

796

797

798 Table 4

799 *Node-pair connections (i.e. edges) that explained a significant portion of variance in RSA and*  
800 *SCL in the regression analyses.* Forward-entry hierarchical regression analyses in 15 patients  
801 with bvFTD and 13 healthy controls (controlling for age, sex, education, and diagnosis) were  
802 used to determine which edges were significant predictors of baseline PANS and SANS. Edges  
803 with positive and negative associations with RSA and SCL entered the models, suggesting that a  
804 combination of strong and weak functional connectivity in the ANS network is necessary for  
805 resting physiological activity. † denotes edge that lost significance when controlling for mean  
806 resting respiration period and inter-beat interval. \* denotes edges that lost significance when  
807 controlling for the mean gray matter volume of the nodes in that edge.

|                             | <i>Edge Category</i> | <i>Edge Label</i> | <i>Zero-order Correlation</i> | $\beta$ | $R^2$ Change | <i>p-value of F Change</i> |
|-----------------------------|----------------------|-------------------|-------------------------------|---------|--------------|----------------------------|
| RSA                         |                      |                   |                               |         |              |                            |
| <i>Positive Correlation</i> |                      |                   |                               |         |              |                            |
|                             | Left vAI –           | 2–5               | .41                           | .48     | .22          | .002                       |
|                             | Left ACC             |                   |                               |         |              |                            |
|                             | Left vAI –           | 2–16              | .33                           | .51     | .14          | .01                        |
|                             | Right ACC †          |                   |                               |         |              |                            |
|                             | Right vAI –          | 13–15             | .29                           | .83     | .12          | .03                        |
|                             | Right ACC            |                   |                               |         |              |                            |

AUTONOMIC NETWORK ARCHITECTURE

|                             |       |      |      |     |      |  |
|-----------------------------|-------|------|------|-----|------|--|
| <i>Negative Correlation</i> |       |      |      |     |      |  |
| Left ACC –                  | 7–9   | -.57 | -.56 | .20 | .01  |  |
| Left Hypothalamus           |       |      |      |     |      |  |
| Left ACC –                  | 7–19  | -.57 | -.52 | .30 | .001 |  |
| Right Hypothalamus          |       |      |      |     |      |  |
| Right ACC –                 | 16–19 | -.33 | -.37 | .12 | .01  |  |
| Right Hypothalamus†         |       |      |      |     |      |  |
| Right vAI1 –                | 12–13 | -.32 | -.61 | .09 | .04  |  |
| Right vAI2                  |       |      |      |     |      |  |
| Right ACC –                 | 17–19 | -.30 | -.43 | .06 | .04  |  |
| Right Hypothalamus*         |       |      |      |     |      |  |
| Right vAI –                 | 13–19 | -.26 | .11  | .21 | .01  |  |
| Right Hypothalamus†*        |       |      |      |     |      |  |
| Right vAI –                 | 12–17 | -.25 | -.32 | .06 | .01  |  |
| Right ACC†                  |       |      |      |     |      |  |
| Left ACC –                  | 6–18  | -.22 | -.42 | .09 | .02  |  |
| Right Amygdala†             |       |      |      |     |      |  |
| SCL                         |       |      |      |     |      |  |
| <i>Positive Correlation</i> |       |      |      |     |      |  |
| Left ACC –                  | 6–19  | .31  | .65  | .14 | .02  |  |
| Right Hypothalamus          |       |      |      |     |      |  |
| Right ACC –                 | 16–18 | .23  | .38  | .08 | .04  |  |
| Right Amygdala              |       |      |      |     |      |  |
| <i>Negative Correlation</i> |       |      |      |     |      |  |
| Left dAI –                  | 1–21  | -.37 | -.54 | .25 | .003 |  |

AUTONOMIC NETWORK ARCHITECTURE

|                    |       |      |      |     |      |
|--------------------|-------|------|------|-----|------|
| PAG                |       |      |      |     |      |
| Right vAI1 –       | 12–13 | -.31 | -.39 | .10 | .03  |
| Right vAI2         |       |      |      |     |      |
| Right ACC –        | 17–5  | -.30 | -.40 | .12 | .01  |
| Left ACC           |       |      |      |     |      |
| Right dAI –        | 11–21 | -.28 | -.71 | .25 | .003 |
| PAG                |       |      |      |     |      |
| Left aMCC –        | 4–19  | -.20 | -.59 | .16 | .02  |
| Right Hypothalamus |       |      |      |     |      |

808

809

Table 5

Edge weight connectivity strength in bvFTD versus healthy controls. Mean connectivity strengths of the edges that entered the RSA and SCL regression models for bvFTD (n=15) and healthy control (n=14) groups.

| Edge Category               | Edge Label | bvFTD<br>M (SD) | Healthy Controls<br>M (SD) | T     | p   |
|-----------------------------|------------|-----------------|----------------------------|-------|-----|
| RSA                         |            |                 |                            |       |     |
| <i>Positive Correlation</i> |            |                 |                            |       |     |
| Left vAI –                  | 2–5        | .40             | .46                        | -1.17 | .25 |
| Left ACC                    |            | (.28)           | (.31)                      |       |     |
| Left vAI –                  | 2–16       | .41             | .49                        | -0.77 | .45 |
| Right ACC                   |            | (.29)           | (.24)                      |       |     |
| Right vAI –                 | 13–15      | .44             | .51                        | -2.42 | .02 |
| Right ACC                   |            | (.29)           | (.28)                      |       |     |
| <i>Negative Correlation</i> |            |                 |                            |       |     |
| Left ACC –                  | 7–9        | .17             | .14                        | -0.01 | .99 |
| Left Hypothalamus           |            | (.31)           | .25)                       |       |     |
| Left ACC –                  | 7–19       | .14             | .20                        | 0.08  | .94 |
| Right Hypothalamus          |            | (.25)           | (.17)                      |       |     |
| Right ACC –                 | 16–19      | .13             | .32                        | 1.43  | .17 |
| Right Hypothalamus          |            | (.24)           | (.19)                      |       |     |

AUTONOMIC NETWORK ARCHITECTURE

|     |                             |       |       |       |       |     |
|-----|-----------------------------|-------|-------|-------|-------|-----|
|     | Right vAI1 –                | 12–13 | .66   | .66   | -0.17 | .87 |
|     | Right vAI2                  |       | (.26) | (.25) |       |     |
|     | Right ACC –                 | 17–19 | .12   | .28   | 0.22  | .83 |
|     | Right Hypothalamus          |       | (.26) | (.18) |       |     |
|     | Right vAI –                 | 13–19 | .20   | .35   | 0.30  | .77 |
|     | Right Hypothalamus          |       | (.24) | (.21) |       |     |
|     | Right vAI –                 | 12–17 | .31   | .33   | -0.73 | .47 |
|     | Right ACC                   |       | (.28) | (.22) |       |     |
|     | Left ACC –                  | 6–18  | .20   | .41   | -2.28 | .03 |
|     | Right Amygdala              |       | (.24) | (.34) |       |     |
| SCL |                             |       |       |       |       |     |
|     | <i>Positive Correlation</i> |       |       |       |       |     |
|     | Left ACC –                  | 6–19  | .11   | .37   | -2.04 | .05 |
|     | Right Hypothalamus          |       | (.23) | (.17) |       |     |
|     | Right ACC –                 | 16–18 | .18   | .39   | -2.14 | .04 |
|     | Right Amygdala              |       | (.18) | (.33) |       |     |
|     | <i>Negative Correlation</i> |       |       |       |       |     |
|     | Left dAI –                  | 1–21  | .06   | .12   | -1.04 | .31 |
|     | PAG                         |       | (.27) | (.32) |       |     |
|     | Right vAI1 –                | 12–13 | .66   | .66   | -0.17 | .86 |
|     | Right vAI2                  |       | (.26) | (.25) |       |     |
|     | Right ACC –                 | 17–5  | .47   | .52   | -2.21 | .04 |
|     | Left ACC                    |       | (.19) | (.25) |       |     |
|     | Right dAI –                 | 11–21 | -.05  | .15   | -2.31 | .03 |
|     | PAG                         |       | (.22) | (.24) |       |     |

AUTONOMIC NETWORK ARCHITECTURE

|                    |      |       |       |       |     |
|--------------------|------|-------|-------|-------|-----|
| Left aMCC –        | 4–19 | .14   | .36   | -2.24 | .04 |
| Right Hypothalamus |      | (.25) | (.22) |       |     |

814

815 Legends

816 Figure 1

817 *Anatomical framework of autonomic functioning and relevant ROIs.* (A) Building on previous  
 818 studies, we developed a lateralized schematic of parasympathetic autonomic nervous system  
 819 (PANS) and sympathetic autonomic nervous system (SANS) functioning. The salience network  
 820 is anchored by hubs in anterior insula (AI) and anterior cingulate cortex (ACC) and has tight  
 821 connections with central pattern generators including the amygdala, hypothalamus, and  
 822 periaqueductal gray. Although this framework does not include many brainstem regions that are  
 823 also integral for ANS activity (e.g., nucleus of the solitary tract, parabrachial nucleus, nucleus  
 824 ambiguus, dorsal motor nucleus of the vagus, and rostral ventrolateral medulla, among others), it  
 825 does include critical cortical and subcortical regions that can be measured with neuroimaging  
 826 techniques. Thus, this represents a simplified yet testable conceptualization of the neural system  
 827 that supports resting physiological activity as well as phasic emotional reactions. (B) We  
 828 extracted the BOLD time series from 21 ROIs that pertained to our neuroanatomical model of  
 829 ANS functioning. Connectivity strength between each node-pair (or edge) was calculated by  
 830 correlating the BOLD time series of each ROI with the BOLD time series of every other ROI,  
 831 which provided us with a matrix of 210 edges to correlate with measures of baseline RSA and  
 832 SCL. The ROIs were functionally connected to the insula and were obtained from task-free fMRI  
 833 data in an independent cohort of healthy older controls. These ROIs (with the numerical labels  
 834 that we assigned to them denoted in parentheses) included: left dorsal AI (1), right dorsal AI  
 835 (11), left ventral AI node 1 (2), right ventral AI node 1 (12), left ventral AI node 2 (3), right  
 836 ventral AI node 2 (13), left anterior midcingulate cortex (4), right anterior midcingulate cortex  
 837 (14), left pregenual ACC node 1 (5), right pregenual ACC node 1 (15), left pregenual ACC node



## AUTONOMIC NETWORK ARCHITECTURE

838 2 (6), right pregenual ACC node 2 (16), left subgenual ACC (7), right subgenual ACC (17), left  
 839 amygdala (8), right amygdala (18), left hypothalamus (9), right hypothalamus (19), left thalamus  
 840 (10), right thalamus (20), periaqueductal gray (21). AI = anterior insula, ACC = anterior  
 841 cingulate cortex, aMCC = anterior midcingulate cortex, Amy = amygdala, dAI = dorsal anterior  
 842 insula, Hyp = hypothalamus, PAG = periaqueductal gray, Thal = thalamus, and vAI = ventral  
 843 anterior insula.

844 Figure 2

845 *Baseline PANS activity is determined by the strength of certain salience network connections*  
 846 *and the suppression of others.* (A) Atrophy in left vAI was associated with lower RSA at  $p <$   
 847 .001, uncorrected (controlling for age, sex, and education) in 21 patients with bvFTD. Cyan  
 848 represents  $T$ -scores at  $p <$  .001, uncorrected ( $T >$  3.69), and green represents  $t$ -scores at  $p <$  .005,  
 849 uncorrected ( $T >$  2.92). (B) We conducted a follow-up VBM analysis of RSA in which we added  
 850 SCL as an additional covariate to the model. The results remained largely unchanged though  
 851 some weaker clusters no longer remained significant. Cyan represents  $T$ -scores at  $p <$  .001,  
 852 uncorrected ( $T >$  3.79), and green represents  $T$ -scores at  $p <$  .005, uncorrected ( $T >$  2.98). (C) The  
 853 fMRI analyses revealed that lower baseline PANS activity was associated with lower vFI – ACC  
 854 connectivity and higher connectivity primarily in ACC – hypothalamus/amygdala. Line  
 855 thickness is scaled to reflect the percentage of variance that each edge explained (i.e.,  $R^2$  change,  
 856 which ranged from .06 to .30) in the hierarchical regression model. Statistical maps are  
 857 superimposed on the Montreal Neurological Institute template brain.

858 Figure 3

Baseline SANS activity is determined by the strength of certain salience network connections and the suppression of others. (A) Atrophy in inferior temporal gyrus, dorsal mid-insula, and hypothalamus was associated with lower SCL at  $p < .001$ , uncorrected (controlling for age, sex, and education) in 20 patients with bvFTD. At more permissive thresholds ( $p < .005$ , uncorrected), smaller volume in the amygdala and PAG was also associated with lower SCL. The inferior temporal gyrus was the only cluster that survived permutation analysis,  $p_{FWE} < .05$ . Cyan represents  $T$ -scores at  $p < .001$ , uncorrected ( $T > 3.73$ ), and green represents  $t$ -scores at  $p < .005$ , uncorrected ( $T > 2.95$ ). (B) We conducted a follow-up VBM analysis of SCL in which we added RSA as an additional covariate to the model. The results remained largely unchanged though some weaker clusters no longer remained significant. Blue represents  $T$ -scores at  $p < .001$ , uncorrected ( $T > 3.79$ ), and green represents  $T$ -scores at  $p < .005$ , uncorrected ( $T > 2.98$ ). (C) Baseline SANS deficits were associated with lower connectivity in right amygdala/hypothalamus edges and higher connectivity primarily in bilateral dAI – PAG edges. Line thickness is scaled to reflect the percentage of variance that each edge explained (i.e.,  $R^2$  change, which ranged from .08 to 25) in the hierarchical regression model. Statistical maps are superimposed on the Montreal Neurological Institute template brain.

Figure 4

*Regression Plots for the Functional Imaging Analyses.* Partial residual plots for the four edges that explained the greatest percentage of variance ( $R^2$  change) in RSA and SCL (controlling for age, sex, education, and diagnosis). Higher resting RSA was associated with (A) greater left vAI – left ACC (edge 2–5) and (B) lower left ACC – right hypothalamus (edge 7–19) functional connectivity. Higher SCL was associated with (C) greater left ACC – right hypothalamus (edge 6–19) and (D) lower right dAI – PAG (edge 11–21) functional connectivity. Given that we

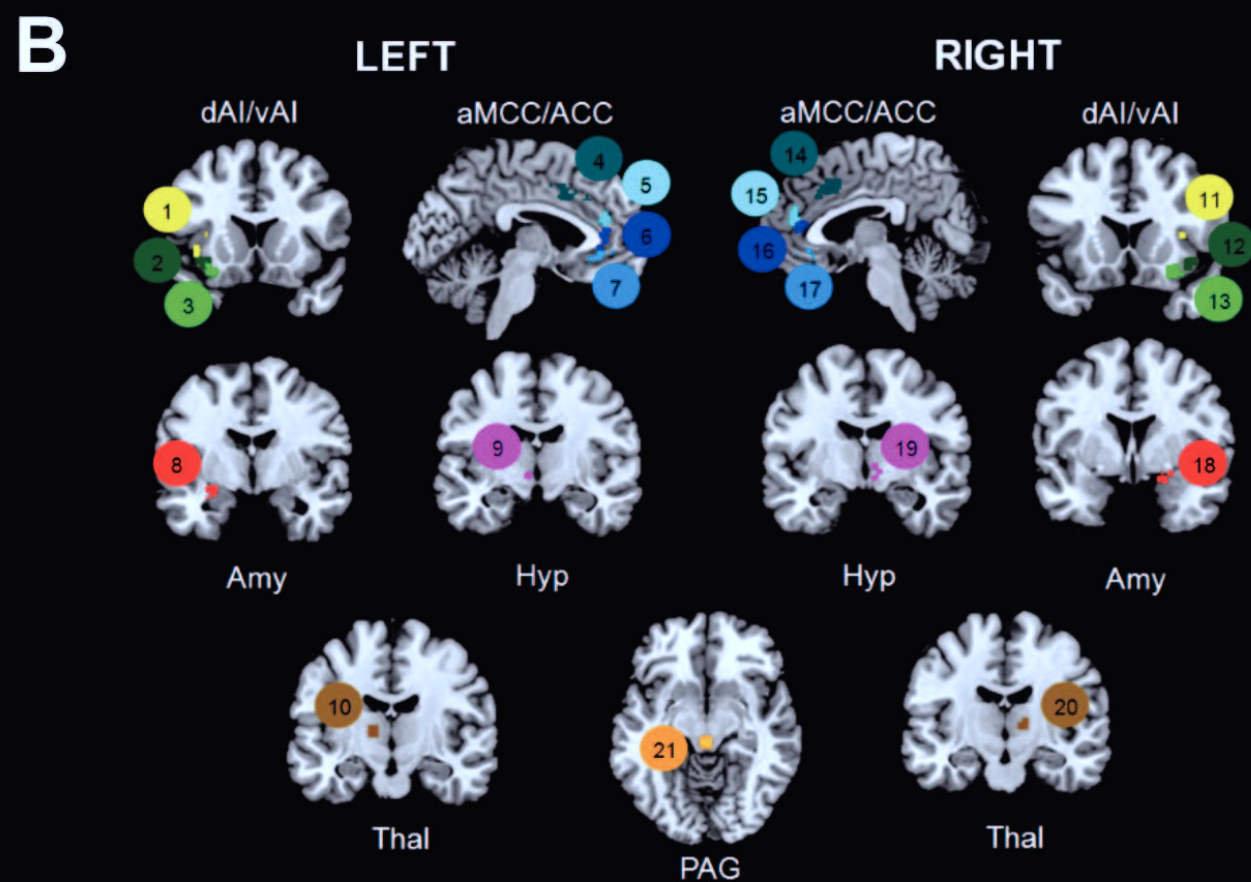
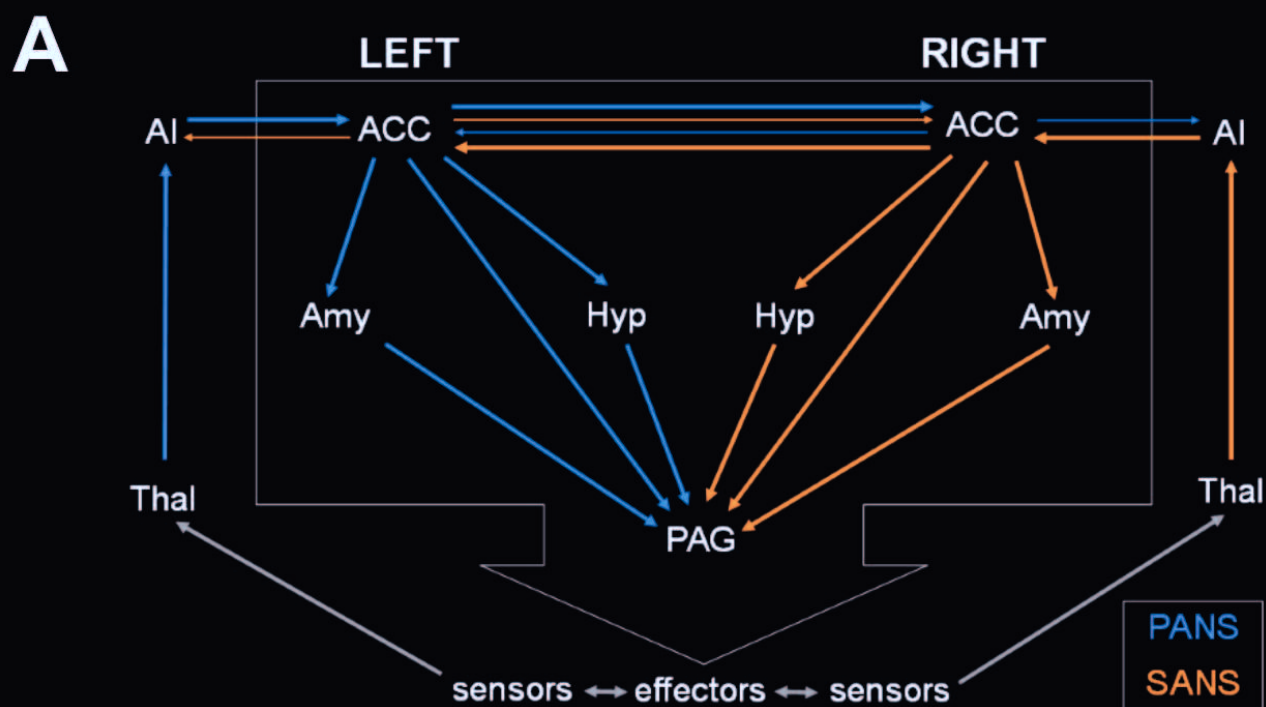
## AUTONOMIC NETWORK ARCHITECTURE

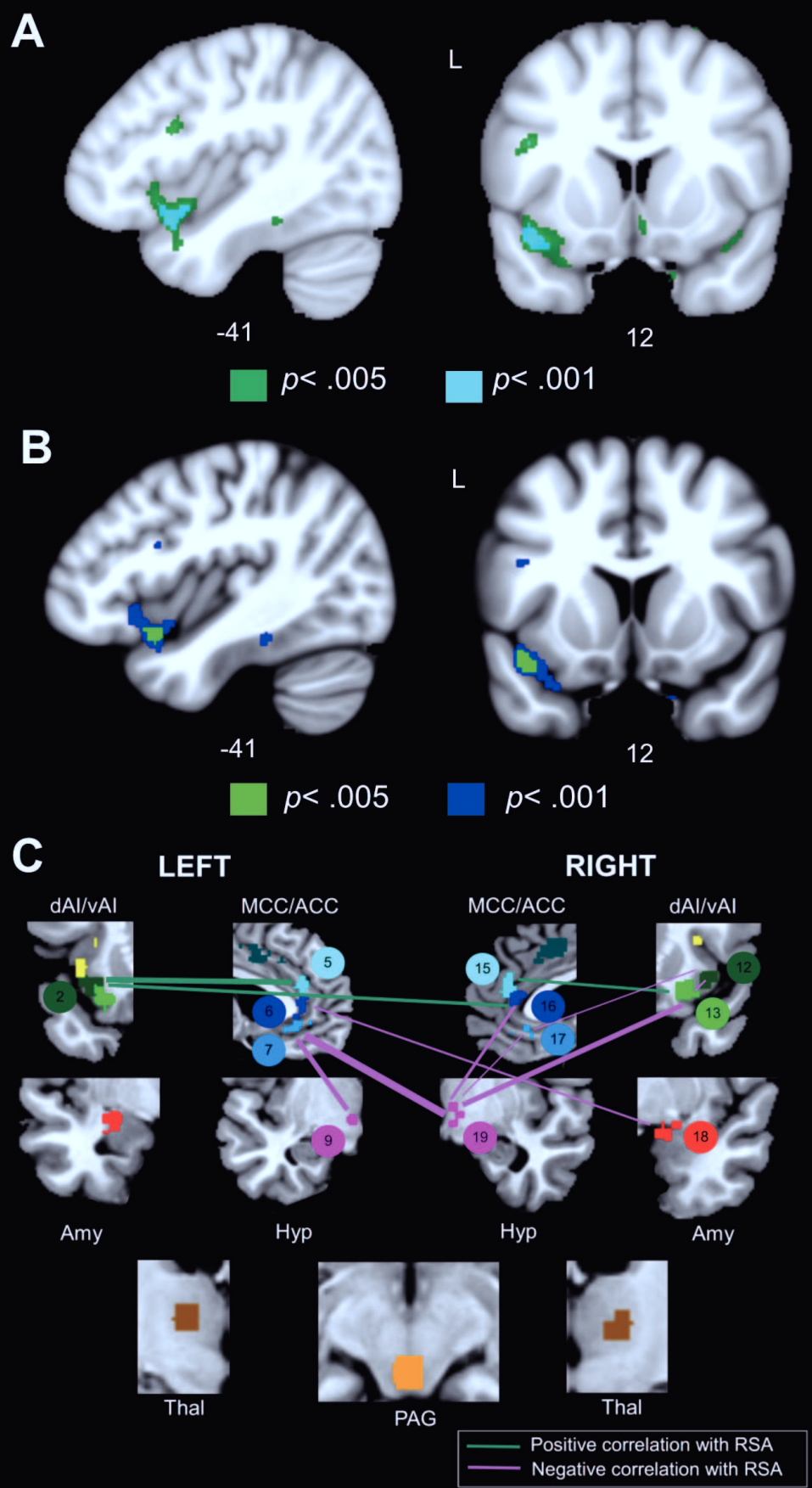
882 controlled for diagnosis in the regression models, these plots show that the association that we  
883 detected between edge connectivity and resting autonomic activity were present in both  
884 diagnostic groups and thus, were not driven by group membership. When we repeated the  
885 original analyses in each diagnosis separately, RSA and SCL had similar associations with the  
886 functional connectivity measures (Figure 4-1). See Figure 1 for abbreviations.

887 Figure 5

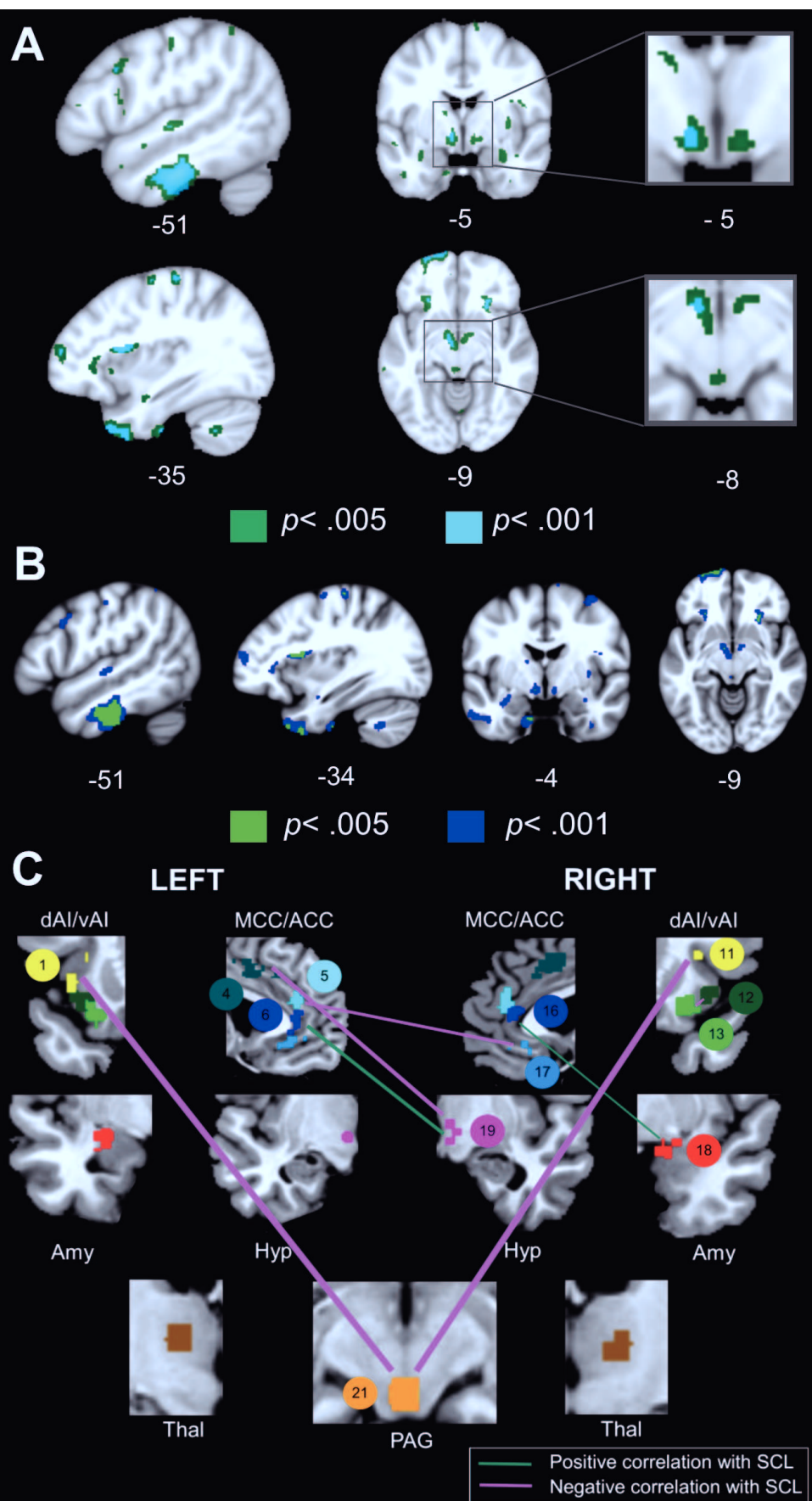
888 *Hypothesized RSA network.* Our results suggest that resting PANS tone depends on the integrity  
889 of both strong and weak edges in the salience network. Stronger vAI – ACC connectivity and  
890 weaker ACC – hypothalamus/amygdala connectivity was associated with higher resting RSA.  
891 RSA, therefore, depends on intact connections between vAI (left > right) and ACC and weaker  
892 connections between ACC and hypothalamus/amygdala (right > left), suggesting that nodes that  
893 support SANS outflow must be inhibited to facilitate PANS activity. We hypothesize that PANS-  
894 specific (e.g., ventrolateral PAG) and SANS-specific (e.g., dorsal PAG) subregions in each node  
895 as well as untested connections with brainstem nuclei that are difficult to image (e.g., nucleus  
896 ambiguus) may also play important roles in this network that we were not able to evaluate. Green  
897 lines are edges in which stronger connectivity promoted RSA (i.e., edges 2–5, 2–16, and 13–15),  
898 and purple lines are edges in which stronger connectivity inhibited RSA (i.e., 13–19, 7–9, 16–19,  
899 17–19, and 6–18). \* indicates edges that emerged as significant predictors of RSA in the  
900 regression models. Laterality has been omitted for visual simplicity but is alluded to in the figure  
901 layout. dPAG = dorsal PAG, vlPAG = ventrolateral PAG. See Figure 1 for other abbreviations.

902

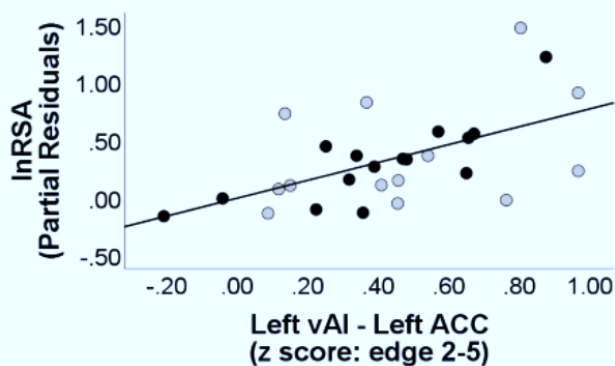




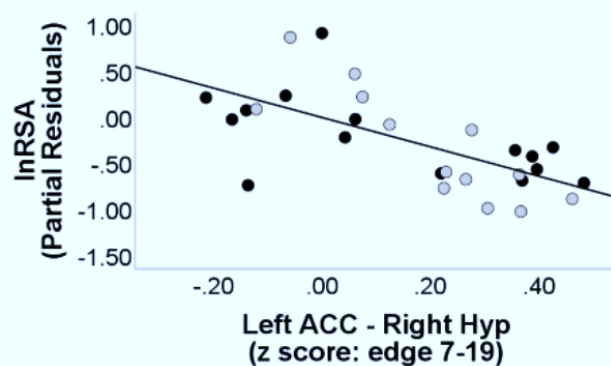




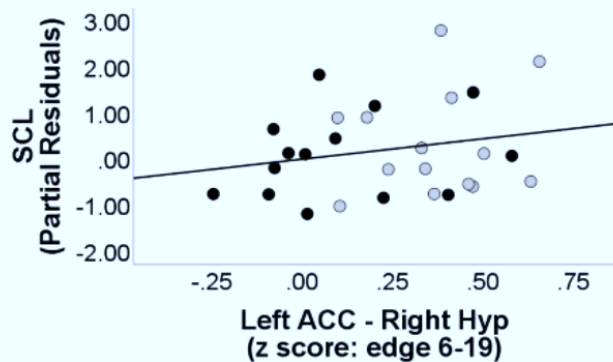
### A Positive Correlation with RSA



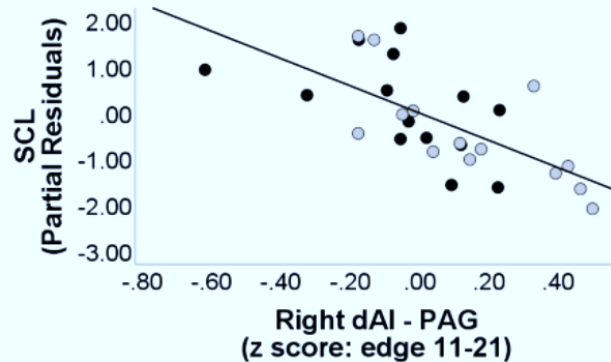
### B Negative Correlation with RSA



### C Positive Correlation with SCL



### D Negative Correlation with SCL



Diagnosis ● bvFTD ● HC

